

# PM<sub>10</sub> within Indian standard is achievable by mitigating the sources of PM<sub>1</sub>: A thirteen years (2009–2021) long study and future prediction (2024) over the eastern Himalayas, India

Abhinandan Ghosh <sup>a</sup>, Monami Dutta <sup>b</sup>, Abhijit Chatterjee <sup>b,\*</sup>

<sup>a</sup> Department of Civil Engineering, Center of Environmental Science and Engineering, IIT-Kanpur, Kanpur, 201086, India

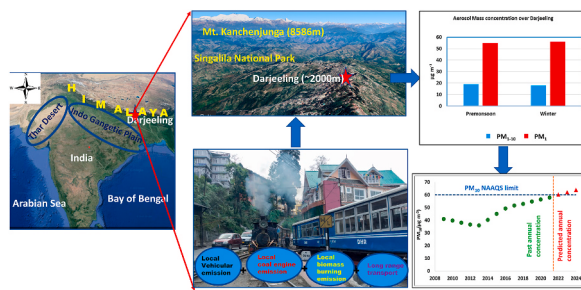
<sup>b</sup> Environmental Sciences Section, Bose Institute, EN Block, Sector-V, Saltlake, Kolkata, 700091, India



## HIGHLIGHTS

- PM10 decreased during 2009–2013 followed by sharp increase since 2014.
- High PM10 over eastern Himalaya is due to high premonsoon and winter-time PM1.
- 80–85% PM1 pollution over eastern Himalaya is contributed by combustion activities.
- PM10 pollution level over eastern Himalaya would cross Indian standard by 2024.

## GRAPHICAL ABSTRACT



## ARTICLE INFO

**Keywords:**  
Eastern Himalaya  
The size distribution of aerosols  
PM<sub>1</sub> aerosol  
Source apportionment  
ARIMA  
Long-term trend

## ABSTRACT

A thirteen years-long (2009–2021) study was conducted on PM<sub>10</sub> pollution over a high-altitude station, Darjeeling (27.1° N and 88.15° E, 2000 m amsl) in the eastern Himalayas in India. To better understand the sources and build a proper mitigation strategy for PM<sub>10</sub>, we have segregated PM<sub>10</sub> into PM<sub>1</sub> and PM<sub>1-10</sub> using the Anderson cascade impactor. A total of 620 sets of samples were collected during the entire study period. PM<sub>10</sub> was found to remain within its Indian standard ( $60 \mu\text{g m}^{-3}$ ) in every year of the study period (long-term average PM<sub>10</sub>:  $46 \pm 8 \mu\text{g m}^{-3}$ ). PM<sub>10</sub> pollution during winter ( $74.0 \pm 15.1 \mu\text{g m}^{-3}$ ) and premonsoon ( $73.1 \pm 12.1 \mu\text{g m}^{-3}$ ) was highest compared to other seasons. Bi-modal mass size distribution of composite PM<sub>10</sub> was observed for all the seasons with maximum peak intensity at the finer mode (PM<sub>1</sub>). Most of the anthropogenic water-soluble ionic components as well as carbonaceous aerosols exhibited maximum intensity at PM<sub>1</sub> too. PM<sub>10</sub> exhibited a steady decrease from 2009 to 2013 but since 2014, a sharp rise was observed. Further, we have observed that premonsoon and winter-time PM<sub>1</sub> pollution was the key factor for a such high rise in PM<sub>10</sub>. PM<sub>1</sub> increased sharply at a rate of  $4.1 \mu\text{g m}^{-3} \text{ yr}^{-1}$  in premonsoon and  $3.3 \mu\text{g m}^{-3} \text{ yr}^{-1}$  in winter since 2014. Auto regressive integrated moving average (ARIMA) model for future prediction revealed that PM<sub>10</sub> would cross its Indian standard and PM<sub>1</sub> alone would cross the PM<sub>2.5</sub> standard in 2024 if the current scenario remains the same and the city would be enlisted among the “non-attainment” cities of the country under “National Clean Air Program (NCAP)” of Government of India. The Positive matrix factorization (PMF) model was run to apportion the sources of PM<sub>1</sub> and PM<sub>10</sub>. It was observed that the vehicular emissions in premonsoon (33% in PM<sub>1</sub>; 28% in PM<sub>10</sub>; contribution of vehicular emission in PM<sub>1</sub> to PM<sub>10</sub> > 90%) and biomass burning in winter (27% in PM<sub>1</sub>;

\* Corresponding author.

E-mail address: [abhijit.boseinst@gmail.com](mailto:abhijit.boseinst@gmail.com) (A. Chatterjee).

23% in  $\text{PM}_{10}$ ; contribution of  $\text{PM}_1$  to  $\text{PM}_{10} > 80\%$ ) are the most influencing sources that need to be curbed to mitigate  $\text{PM}_1$  and hence  $\text{PM}_{10}$  pollution over Darjeeling.

## 1. Introduction

Standing on 2023, we are well cognizant of the role of aerosols on weather and climate and human health (Pope et al., 2009; Cesari et al., 2016; Pope et al., 2004; Pope and Dockery, 2006; Li and Shao, 2009; Jain et al., 2017; Cesari et al., 2018). Amid several other policies, the Government of India has taken a new challenge to combat air pollution in the country, and very recently in 2019; it launched a national mission called “National Clean Air Program (NCAP)” for the same. A total of 131 cities have been found that do not meet the national ambient air quality standard (NAAQS) of India for various air pollutants, especially aerosols,  $\text{PM}_{2.5}$  and  $\text{PM}_{10}$ . However, NCAP is mainly focused on polluted metro-cities and urban agglomeration but does not cover non-urban atmospheres. Recently, Ravishankara et al. (2020) had clearly shown that air pollution in India is not only an urban problem. Several regions hold immense importance from the point of view of human health as well as climatically, geographically, and ecologically where air pollution is an issue but has not yet emerged distinctly or come into the sight of bureaucrats or decision-makers.

The high-altitude Himalayan urban atmospheres are such an example. If we look at the long-term annual average data, we find that  $\text{PM}_{2.5}$  and  $\text{PM}_{10}$  meet NAAQS and therefore these regions are not considered as polluted. However, in a country like India, phenomenal inter-seasonal variability of meteorological conditions plays a crucial role in pollution accumulation or dispersion (Ghosh et al., 2021). Hence, with changes in seasonal meteorological conditions attainment and non-attainment criteria can be rapidly altered in some places.

In this study, we have conducted thirteen years long (2009–2021) study on size-segregated  $\text{PM}_{10}$  over Darjeeling which represents a high-altitude urban atmosphere of the eastern Himalayas. The study has mainly three-fold objectives. First, we have discussed the long-term seasonal variability and mass size distribution of aerosol and its different components. Secondly, we have discussed the long-term trend of size-segregated aerosols and estimated the rate of change in concentration of size-segregated aerosols over the years for the polluted seasons. We have also predicted the future concentration of  $\text{PM}_{10}$  and  $\text{PM}_1$  for 2024 under the Business-As-Usual (BAU) scenario to draw the attention of policymakers to implement immediate strategic action plans to curb air pollution over this part of the Himalayas. Thirdly, to provide preliminary background information to formulate action plans to control air pollution over Darjeeling, we have investigated the potent source regions and all plausible sources of the most contributing size regimes in the  $\text{PM}_{10}$  aerosols using trajectory and source receptor models. This will help to implement a more accurate and cost-effective policy which will be beneficial for both financial and climatic prospects. The such long-term and in-detail study would make the scientific community to better realize the importance of jointly exploring the size, chemistry, and seasonality of aerosols for framing better mitigation policies rather than exploring composite aerosols.

## 2. Site description

Darjeeling ( $27.1^\circ \text{N}$  and  $88.15^\circ \text{E}$ ,  $\sim 2000 \text{ m amsl}$ ) is a high-altitude urban atmosphere situated over the eastern Himalayas and is a world-famous tourist spot for its majestic view of Mt. Kangchenjunga and valleys. Geographically and climatically the eastern Himalayas exhibited phenomenal variability. The southern foothills suddenly rise from the plains from a height of about 100 m to reach 1500 m. East-west elongated inner valleys, also called ‘dun valleys’, are densely populated. The first orographic barrier of the outer Himalayas, also called the Mahabharat range, rises rapidly to about 3000 m. The topography of the

area is rugged and steeper in the western part than in the eastern part. The Darjeeling township is situated in the Mahabharat range. The relatively mature and subdued geomorphic zone to the north of the Mahabharat Range is known as the Midland zone with an altitude of the area varies from 200 to 2500 m. and further north the Fore Himalayas with altitudes ranging from 2500 to 4000 m. The region is heavily influenced by south east monsoon and with wet summer and dry cold winter. Although, the latitudinal extent of the region is located within the sub-tropical climatic regime, its mountainous configuration has led to varied climates ranging from subtropical to temperate and alpine type. The Darjeeling Township is situated nearly 70 km from the nearest point of the Indo-Gangetic Plain (IGP). The city consists of numerous numbers of hotels, restaurants, and market complexes with a high density of tourist vehicles on the road. The sampling location is situated at an elevation of 200 m from the main township and is covered with deep vegetation. The nearest road with significant vehicular activity is about 200 m away from the study site. Several major and minor tea gardens are situated within the  $\sim 10\text{--}12 \text{ km}$  radius of the sampling location. More details about the site along with geographical location, topographical features, and urban agglomeration can be found elsewhere (Chatterjee et al., 2010; Chatterjee et al. 2012; Adak et al., 2014; Roy et al., 2017; Roy et al., 2019; Sarkar et al., 2019; Chatterjee et al., 2020; Ghosh et al., 2020; Sharma et al. 2020; Chatterjee et al., 2021; Sharma et al. 2021; Ghosh et al., 2021; Rai et al., 2021; Mukherjee et al., 2022; Dutta et al., 2023).

## 3. Methodology

### 3.1. Collection of aerosols

Aerosol samples were collected using a nine-stage Anderson cascade impactor on weekly basis for thirteen consecutive years (2009–2021). Samples of three phases were excluded from the study as there was no business-as-usual scenario over the study area (May–October 2017 because of political agitations; March–August 2020 and May–July 2021 due to covid –19 lockdown). A total of 620 sets of size-segregated aerosol samples were studied during the entire study period covering all the seasons ( $n = 142$  for premonsoon, 218 for monsoon, 104 for postmonsoon, and 156 for winter). There are nine size fractions with aerodynamic cut-off diameters of 0.4, 0.7, 1.1, 2.1, 3.3, 4.7, 5.8, 9, and 10  $\mu\text{m}$  in the Anderson cascade impactor. Pre-baked quartz filter papers were used as the impaction substrates to collect the aerosols. The instrument was run continuously for 72 h (12:00 IST–12:00 IST) for adequate deposition with a constant flow rate of 27.3 LPM to obtain maximum efficiency. All the impaction substrates were weighed immediately before and after each sampling following a 24 h equilibration inside a constant temperature ( $25^\circ \text{C}$ ) and humidity ( $\sim 40\%$ ) chamber. Thereafter the total deposition of aerosols ( $\mu\text{g}$ ) was divided by the volume of air ( $\text{m}^3$ ) drawn to calculate the aerosol concentrations.

### 3.2. Analysis of water-soluble ionic species

After the sampling, the filter papers were cut into two halves. The first half was extracted and ultra-sonicated in 20 ml Milli-Q water ( $18.2 \text{ M}\Omega$  resistivity) for 30 min. The extract was then filtered and stored at  $4^\circ \text{C}$  in the refrigerator before the chemical analysis. Water-soluble inorganic ions ( $\text{Na}^+$ ,  $\text{NH}_4^+$ ,  $\text{K}^+$ ,  $\text{Ca}^{2+}$ ,  $\text{Mg}^{2+}$ ,  $\text{Cl}^-$ ,  $\text{NO}_3^-$  and  $\text{SO}_4^{2-}$ ) were measured by an ion chromatograph (861 Advanced Compact IC, Metrohm, Switzerland). The details of the chromatographic analysis can be found in our earlier study (Ghosh et al., 2021). The detection limits for the water-soluble ionic species were 0.05, 0.06, 0.08, 0.06, 0.08, 0.6,

0.4, and 0.07 ppm for  $\text{Na}^+$ ,  $\text{NH}_4^+$ ,  $\text{K}^+$ ,  $\text{Ca}^{2+}$ ,  $\text{Mg}^{2+}$ ,  $\text{Cl}^-$ ,  $\text{NO}_3^-$  and  $\text{SO}_4^{2-}$  respectively. The analytical precision of the ions was computed from repeated measurements running standard samples of ionic species. The precision was found to be 3% for  $\text{SO}_4^{2-}$  and 2% for the rest of the ions.

### 3.3. Analysis of the carbonaceous components

The concentrations of organic and elemental carbon (OC and EC) in size segregated samples were measured by OC/EC carbon analyzer (Model: DRI 177 2001A; Make: Atmoslytic Inc. Calabasas, CA, USA) using IMPROVE-A Protocol (Chow et al., 2004). OC/EC carbon analyzer is working on the preferential oxidation of OC and EC at different temperatures plateaus (140, 280, 480, and 181 580 °C, for OC1, OC2, OC3, and OC4, respectively) in pure helium and three temperature plateaus (580, 740, and 840 °C for EC1, EC2, and EC3, respectively) in 98% helium and 2% 184 oxygen mixture (Chow et al., 2004). A punch of

$$\text{Unc} = \text{Max} \left( \frac{\sqrt{((\text{Blank ion} + \text{Conc of Ion} * \text{Del relativity}^2) + \text{Sample unc}^2 + \text{Conc of ions}^2)}}{\text{sample vol}}, \sigma \right) \quad (\text{Eq. 3})$$

~0.536 cm<sup>2</sup> area of the filter was taken and analyzed along with the field blank filters. The repeatability error of OC and EC analysis was estimated as 3–7%. More details on OC/EC analysis can be found elsewhere (Sharma et al. 2021).

### 3.4. Positive Matrix Factorization (PMF) model for source apportionment of aerosols

Positive Matrix Factorization (PMF) is a statistical modelling technique and a multivariate statistical tool widely used for the source apportionment of atmospheric aerosols (Paatero and Hopke, 2003; Gupta et al., 2012; Cesari et al. 2016; Massey et al., 2016; Sharma et al., 2016; Gadi et al., 2019; Ray et al., 2019). It requires a comprehensive dataset of samples and associated uncertainty as inputs and gives several variables such as factor profiles, their contribution and error in modeling as output (Polissar et al., 1998; Paatero and Hopke, 2003; Pakbin et al., 2011; Paatero et al., 2002).

Thus, the chemically speciated aerosol samples were assembled as a data matrix 'X' of i x j dimensions, in which i is the number of samples and j is the number of chemical species measured during analysis. The model is based on the chemical characterization of the collected aerosols aimed to solve Eq. (1).

$$X_{ij} = \sum_{k=1}^p g_{ik} f_{jk} + e_{ij} \quad (1)$$

where p is the number of factors contributing to the ambient aerosols,  $x_{ij}$  is the jth compound concentration measured in the ith sample,  $g_{ik}$  is the gravimetric concentration of the jth element in material from the kth source, and  $f_{jk}$  is the airborne mass concentration ( $\mu\text{g}/\text{m}^3$ ) of material from the kth source contributing to the ith sample and  $e_{ij}$  is the residual for each species (difference between the measured and calculated amount). PMF provides a weighted least square problem in which a certain number of factors have to be determined to minimize an 'object function' as shown in Eq. (2). Factor contributions and profiles are calculated by minimizing the object function 'Q' in the PMF model. Q is a significant parameter in the PMF model for which two values, Q (true) and Q (robust), are calculated in the model results. The apportionment technique relies on many trial attempts to arrive at an acceptable solution (Reff et al., 2007; Jiang et al., 2015). More descriptions and technical details can be found elsewhere (Paatero and Hopke, 2003; Pakbin et al., 2011; Jiang et al., 2015).

$$Q = \sum_{i=1}^n \sum_{j=1}^m \left( \frac{x_{ij} - \sum_{k=1}^p g_{ik} f_{kj}}{u_{ij}} \right)^2 \quad (2)$$

Where  $u_{ij}$  is an estimate of the uncertainty of the jth variable in ith sample.

PMF model requires two input files: the 'Concentration' file and the 'Uncertainty' file. As the PMF works on the non-negative aspect, the concentration of any species below the detection limit or zero is replaced by 0.5 x Minimum Detection Limit (MDL) of that species. The uncertainty for measured values of ionic and carbonaceous species was calculated with Eq. (3) (Yan et al., 2017). This calculation includes field as well as analytical uncertainty. If the value of uncertainty was missing, it was replaced by  $(\frac{5}{6} \text{ MDL})$  (Wei et al., 2014).

Where, Unc = Uncertainty of ion, ( $\mu\text{g}/\text{m}^3$ ); Blank ion = Respective ion in Blank, filter ( $\mu\text{g}/\text{ml}$ ); Conc of ion = Concentration of ion, ( $\mu\text{g}/\text{m}^3$ ); Del relativity = Delta Relativity ~ 5%, Smp Unc = Sampling uncertainty ~5%; Smp vol = Respective Sampling volume, ( $\text{m}^3$ );  $\sigma$  = Standard Deviation of analytical methods, ( $\mu\text{g}/\text{m}^3$ ). The detailed data screening process is given in the supplementary section.

### 3.5. Autoregressive integrated moving average (ARIMA) for future projection

The future projection was performed with the Box Jenkins Autoregressive Integrated Moving Average (ARIMA) model (Box et al., 1994; Box and Jenkins, 1976). ARIMA model generates time series forecasting for the future using three steps: identification, estimation, and diagnostic checking (Soni et al., 2014). Stationarity in the time series is always checked before proceeding with the ARIMA model. ARIMA model involves two equations:

$$y(t) = \beta + \phi_1 Y_{t-1} + \phi_2 Y_{t-2} + \dots \phi_p Y_{t-p} + \varepsilon_t \quad (\text{Eq. 4})$$

where  $\varepsilon_t$  is white noise. It is represented as AR (p) model, an autoregressive of order P. Here  $\phi_1$ ,  $\phi_2$ ,  $\phi_p$  are the AR coefficients.

$$y(t) = C + \varepsilon_t + \theta_1 \varepsilon_{t-1} + \theta_2 \varepsilon_{t-2} + \dots + \theta_q \varepsilon_{t-q} \quad (\text{Eq. 5})$$

Where  $\varepsilon_t$  is white noise. We refer to this as an MA (q) model representing a moving average model of order q. Here  $\theta_1$ ,  $\theta_2$ ,  $\theta_q$  are the MA coefficients.

ARIMA is the assimilation of AR and MA and the integrated part is represented as differencing term denote as d. ARIMA (p,q,d) model denotes the order of auto-regressive, differencing, and moving average respectively. The best fit ARIMA model for a time series was selected depending on the lowest Akaike's Information Criteria (AIC) and Bayesian Information Criteria (BIC) values. The model robustness was tested by Ljung – the box test through a significant p-value. Before ARIMA analysis the time series PM<sub>1</sub> data was split into training (2009–2019) and validation set (2020–2021) and future projection was performed up to 2024.

### 3.6. Concentration Weighted Trajectory model

5-day air-mass back trajectories, culminating over the sampling locations have been calculated for all the sampling days using the HYSPLIT-4 model developed by NOAA, USA (Draxler et al., 2016). One trajectory was computed per day at 12:00 UTC. We have also performed Concentration Weighted Trajectory (CWT) analysis using Trajstat (Version – 1.4.4) to compare the contributions of various long distant source regions for aerosols (Wang et al., 2009). For CWT analysis, we have used the back trajectories obtained from the HYSPLIT model. In this method, each grid cell was assigned to a weighted concentration by using the following equation derived by Hsu et al. (2003):

where  $C_{ij}$  is the average weighted concentration in the  $i$ th cell,  $l$  is the index of the trajectory,  $M$  is the total number of trajectories,  $C_l$  is the concentration observed on the arrival of trajectory  $l$ , and  $t_{ijl}$  is the time spent in the  $i$ th cell by trajectory  $l$ . The concentration assigned to each grid was determined by the concentration observed on the arrival of the trajectory and the times spent on that particular grid cell.

### *3.7. Vertical profiling of aerosol layer over the eastern Himalaya: observations from CALIPSO*

The Cloud-Aerosol Lidar with Orthogonal Polarization (CALIOP) has two LIDARs and provides information about the aerosol profiling of the troposphere and lower-stratosphere since May 2006 (Winker et al., 2009). It is the primary onboard instrument of the Cloud-Aerosol Lidar and Infrared Pathfinder Satellite Observations (CALIPSO) satellite. The aerosol types classified in the CALIPSO aerosol model are smoke (biomass burning), polluted dust (mixtures of dust and smoke), dust, polluted continental, clean continental, clean marine, volcanic ash, and sulfate. The vertical profile of the aerosol was obtained using CALIOP over the stations during different seasons. More details can be found in Omar et al. (2009).

### 3.8. Active fire count

We have used MODIS collection 6 data to obtain the active fire spots over India during the sampling periods. MODIS Collection 6 data provides the best available active fire products with high efficiency in detecting small fires, improved cloud masking, and expanded sunlight rejection. Data above the confidence level of  $\geq 80\%$  were taken and plotted using open-source GIS software.

#### 4. Results and discussion

#### **4.1. Long-term seasonal variability and mass size distribution of PM<sub>10</sub> aerosols over Darjeeling**

The annual average concentration of composite PM<sub>10</sub> aerosols over Darjeeling was found to be  $46 \pm 8 \mu\text{g m}^{-3}$  for the entire study period (2009–2021) which did not exceed the NAAQS reference value of  $60 \mu\text{g m}^{-3}$ . However, it exhibited distinct seasonal variation (Fig. 1a) with the highest loading during the winter ( $74.0 \pm 15.1 \mu\text{g m}^{-3}$ ) and premonsoon ( $73.1 \pm 12.1 \mu\text{g m}^{-3}$ ) followed by postmonsoon ( $24.8 \pm 3.5 \mu\text{g m}^{-3}$ ) and minimum during monsoon ( $12.9 \pm 1.2 \mu\text{g m}^{-3}$ ). Such seasonal behavior of PM<sub>10</sub> is consistent over the years as observed from our earlier study conducted a decade ago (Chatterjee et al., 2010) as well as in the very recent past (Ghosh et al., 2021). The massive influence of tourist activities (fossil fuel and biomass burning), and the contribution of low-land plain regions by up-slope valley winds are the major sources of aerosol pollution in premonsoon over the site (Chatterjee et al., 2012a, 2012b). On the other hand, during winter, the local biomass burning in addition to the usual local-level anthropogenic activities is the major contributor of aerosols (Ghosh et al., 2021; Mukherjee et al., 2022). High precipitation during the monsoon and postmonsoon period wash off the ground-level aerosols, leading to low concentrations of PM<sub>10</sub>.

To investigate the size regimes with high or significant contributions to total PM<sub>10</sub>, we have performed the analysis of the mass size distribution of cumulative PM<sub>10</sub> aerosols over different seasons as shown in Fig. 1b. During premonsoon a sharp and tall peak was observed at 1.1 µm–0.7 µm over Darjeeling followed by a relatively smaller peak for the larger size particles (4.7 µm–3.3 µm). Darjeeling experiences regional as well as local anthropogenic pollution plumes during the premonsoon (Chatterjee et al., 2010; Ghosh et al., 2021; Mukherjee et al., 2022). Premonsoon is the most common period for tourist activity for this hill station. Thus, the sharp peak at (1.1 µm–0.7 µm) during premonsoon could be attributed to the local vehicular emissions, emissions from the hotel or road side eateries as well as from the regional transport. Up-slope valley wind could also be the reason for the obtained peak at the 1.1 µm–0.7 µm during premonsoon as also observed in previous studies (Ghosh et al., 2021). The peak at the coarse mode (4.7 µm–3.3 µm) during the premonsoon could be associated with non-tailpipe emissions such as road or construction dust due to high prevailing wind speed (Table S3) along with high on-road vehicular activity (Karar and Gupta, 2006).

A sharp fall in both fine and coarse mode particles was observed during monsoon due to in-cloud/below-cloud scavenging. The small coarse size peak of  $5.8 \mu\text{m}$ – $4.7 \mu\text{m}$  could be associated with the transported sea salts from the Bay of Bengal (Ghosh et al., 2020), whereas the fine mode peak between the  $1.1 \mu\text{m}$ – $0.7 \mu\text{m}$  could be associated with the local domestic and vehicular emission (Ghosh et al., 2020). Bi-modal distribution was also observed during the postmonsoon with a flat peak at the fine mode ( $0.7 \mu\text{m}$ – $0.4 \mu\text{m}$ ) and a very little peak at the  $5.8 \mu\text{m}$ – $4.7 \mu\text{m}$ . The fine mode peak could be associated with the new particle formed from the VOCs (Sarkar et al., 2017; Ghosh et al., 2021) or

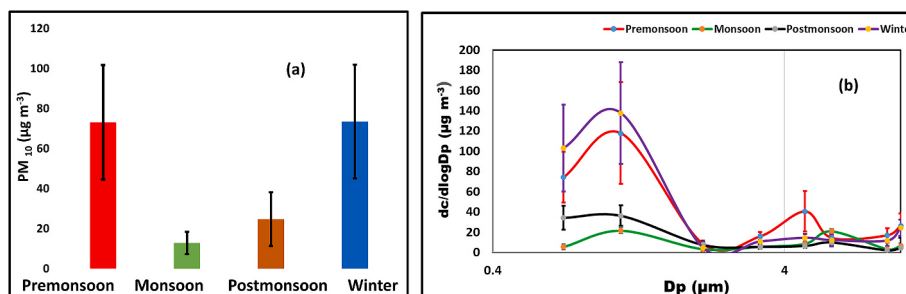


**Fig. 1.** Seasonal Variability of  $\text{PM}_{10}$  (a) and mass size distribution of  $\text{PM}_{10}$  aerosols (b) over Darjeeling

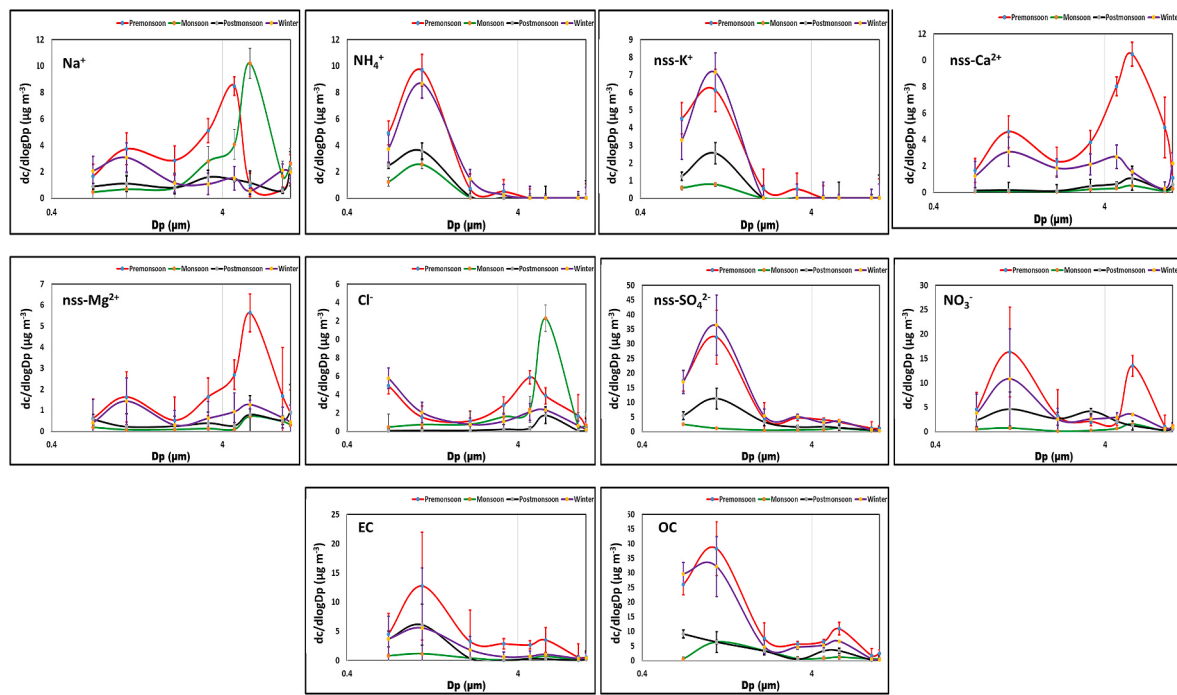


**Fig. 2.** Mass-size distribution of different chemical components of  $\text{PM}_{10}$  over Darjeeling. (Red = premonsoon, Green = monsoon, Black = postmonsoon, and Violet = winter).

from local vehicular emission (Ghosh et al., 2021) while the small coarse peak could be due to soil and road dust. Winter also exhibited a bi-modal distribution with a sharp and most intense fine mode peak at  $1.1 \mu\text{m}$ – $0.7 \mu\text{m}$ . This sharp peak could be associated with local biomass burning as it is a common trend for local people to combat the cold during winter. The accumulation of aerosol further gets facilitated by low wind speed and lesser mixing height depth (Table S3) as well for the thermal inversion and frequent occurrence of ground-level clouds (Chatterjee et al., 2010). Regional transport from the IGP could also contribute to the elevated fine-mode aerosols during the season (Ghosh et al., 2021; Mukherjee et al., 2022). A flat, broad, and low peak of  $10 \mu\text{m}$ – $4.7 \mu\text{m}$  was also observed at the coarse mode and could be associated with the vehicle-driven road dust.

#### 4.1.1. Mass size distribution of various chemical components of $\text{PM}_{10}$ over Darjeeling

The mass size distribution of the various chemical components is shown in Fig. 2 for different seasons over Darjeeling. Among the primary cations,  $\text{Na}^+$  exhibited a unimodal coarse mode peak at  $5.8 \mu\text{m}$ – $4.7 \mu\text{m}$  with a strong association with  $\text{Cl}^-$  ( $R^2 = 0.72$ ) during monsoon, indicating their common source of sea salt (Ghosh et al., 2021) attributed to the influence of marine air masses (Fig. S4). The peak shifted towards  $4.7 \mu\text{m}$ – $3.3 \mu\text{m}$  with an additional smaller peak at  $1.1 \mu\text{m}$ – $0.7 \mu\text{m}$ . The peaks of  $\text{Na}^+$  during premonsoon could be associated with the soil-dust aerosols (Parrington et al., 1983; Matawle et al., 2015) from the IGP along with the impact of marine air masses, though fewer than monsoon. The winter-time fine mode peak at  $1.1 \mu\text{m}$ – $0.7 \mu\text{m}$  could also be attributable to long-range dust transport from IGP as observed in Fig. S4. A prominent bi-modal (large peak at  $5.8 \mu\text{m}$ – $4.7 \mu\text{m}$  and a smaller peak at  $1.1 \mu\text{m}$ – $0.7 \mu\text{m}$ ) mass size distribution pattern was observed for  $\text{nss-Ca}^{2+}$  and  $\text{nss-Mg}^{2+}$  during premonsoon and could be related to the regional and long-distant transported dust aerosols from the arid or semi-arid regions of western India (Kumar and Sarin, 2010). The dust from IGP could also be the reason behind the winter-time peak at  $1.1 \mu\text{m}$ – $0.7 \mu\text{m}$  (Fig. S4). Strong association ( $R^2 > 0.8$ ) of coarse mode  $\text{nss-Mg}^{2+}$  with  $\text{nss-Ca}^{2+}$  was observed during the premonsoon and winter suggesting their common crustal source. The  $\text{nss-K}^+$  is considered

an excellent tracer of biomass burning (Andreae, 1983; Duan et al., 2004; Chatterjee et al., 2010; Ghosh et al., 2019). Uni-modal distribution of  $\text{nss-K}^+$  was observed during the premonsoon and winter with almost identical peak intensity at  $0.7 \mu\text{m}$ – $0.1 \mu\text{m}$ . The regional biomass burning plume could be the reason for the fine mode peak of  $\text{nss-K}^+$  during the premonsoon (Ghosh et al., 2021), while the local biomass burning could be the possible reason for such elevated  $\text{nss-K}^+$  peak during the winter (Chatterjee et al., 2010; Ghosh et al., 2021).

$\text{Cl}^-$  shows a collocated peak with  $\text{Na}^+$  at  $5.8 \mu\text{m}$ – $4.7 \mu\text{m}$  during monsoon indicating their common sources of sea salt. A sharp increase in  $\text{Cl}^-$  is also observed at  $0.7 \mu\text{m}$ – $0.4 \mu\text{m}$  during premonsoon and winter which could be associated with the coal burning for the Darjeeling Himalayan Railways and several hotels/resorts associated with the tourist activities. Among the secondary species,  $\text{nss-SO}_4^{2-}$  was found to be the most abundant with maximum concentration in fine mode with a peak at  $1.1 \mu\text{m}$ – $0.7 \mu\text{m}$  in all the seasons. The local coal burning emission along with the advection from the low-land regions driven by the up-slope valley wind could supply enough  $\text{SO}_2$  over Darjeeling during the premonsoon which could have undergone enhanced photochemical oxidation favored by higher temperatures and stronger solar radiation to form  $\text{nss-SO}_4^{2-}$  (Chatterjee et al., 2010; Ghosh et al., 2021). During the winter the emission of  $\text{SO}_2$  from the local coal combustion and biomass burning for domestic heating (Roy et al., 2017) along with the low level cloud could facilitate the aqueous phase oxidation of  $\text{SO}_2$  to  $\text{SO}_4^{2-}$ , leading to high peak intensity in the fine mode. The smaller and flat peak ( $4.7 \mu\text{m}$ – $2.1 \mu\text{m}$ ) of  $\text{nss-SO}_4^{2-}$  during the entire dry season could be due to the absorption of  $\text{H}_2\text{SO}_4$  onto the dust particles. Nitrate shows a bimodal distribution pattern with sharp peaks at  $1.1 \mu\text{m}$ – $0.7 \mu\text{m}$  in all the seasons (except monsoon) which indicates the high influence of tourist-related vehicular activities. A relatively smaller peak of  $\text{NO}_3^-$  was observed at coarse mode ( $5.8 \mu\text{m}$ – $4.7 \mu\text{m}$ ) during premonsoon when  $\text{NH}_4\text{NO}_3$  could partially get decomposed producing  $\text{HNO}_3$  vapors (Tanner, 1982; Wang et al., 2005) followed by a reaction with soil dust particles ( $R^2 > 0.7$  for the regression analysis between  $\text{Ca}^{2+}/\text{Mg}^{2+}$  and  $\text{NO}_3^-$ ).  $\text{NH}_4^+$  showed a distinct unimodal size distribution pattern with a peak at  $1.1 \mu\text{m}$ – $0.7 \mu\text{m}$  in all the seasons. The similar mass size distribution pattern of  $\text{NH}_4^+$  and  $\text{SO}_4^{2-}$  for the fine mode aerosols with strong correlation ( $R^2 > 0.8$ )

indicates the possible abundance of  $[(\text{NH}_4)_2\text{SO}_4]$  or  $[\text{NH}_4\text{HSO}_4]$  in the atmosphere of Darjeeling. The common sources of  $\text{NH}_3$  are coal combustion, agricultural activity, livestock farming, and biomass burning (Bouwman et al., 1997) which are common in Darjeeling.

Among the carbonaceous aerosols EC and OC exhibited a prominent taller and sharper peak at  $1.1 \mu\text{m}$ - $0.7 \mu\text{m}$  almost in all the dry seasons. Local biomass burning during winter and elevated vehicular activities related to tourists could lead to high fine mode peaks. While the fine mode OC could be attributable to various combustion sources and secondary organic aerosol formation, the coarse mode peaks could be due to the adsorption of OC on the dust particles during aging (Sarkar et al., 2017; Ray et al., 2019; Ghosh et al., 2021).

Overall, the mass distribution analysis revealed that the cumulative PM<sub>10</sub> aerosols as well as its major anthropogenic chemical components (water-soluble ions and carbonaceous) were highly accumulated within ~1 μm (PM<sub>1</sub>). This encouraged us to perform an analysis to compare the loading of highly polluted PM<sub>1</sub> with the other fraction of PM<sub>10</sub> i.e. PM<sub>2.5</sub>-PM<sub>10</sub>.

#### 4.1.2. Relative pollution of $PM_1$ with respect to $PM_{1-10}$

We have compared the loading of PM<sub>1</sub> with PM<sub>1-10</sub> over different seasons as shown in Fig. 3. It can be seen that during the two highly polluted seasons (premonsoon and winter), PM<sub>1</sub> was 2.5–3 times higher than PM<sub>1-10</sub>. Therefore, PM<sub>1</sub> is the key fraction of PM<sub>10</sub> that was responsible for the high loading of PM<sub>10</sub> during the polluted seasons; premonsoon and winter. As the carbonaceous components are the major contributor of PM<sub>10</sub> aerosol over Darjeeling (Chatterjee et al., 2021; Ghosh et al., 2021), we have checked the relative loading of carbonaceous components between PM<sub>1</sub> and PM<sub>1-10</sub> and discussed below.

#### 4.1.3. Carbonaceous components in $PM_1$ and $PM_{1-10}$

The seasonal variabilities of EC, OC, and the estimated secondary organic carbon (SOC) in PM<sub>1</sub> and PM<sub>1-10</sub> have been shown in Fig. 4. The average concentration of EC in PM<sub>10</sub> over Darjeeling was found to be  $4.2 \pm 2.1 \mu\text{g m}^{-3}$ , with maximum concentration during the premonsoon ( $7.1 \pm 1.1 \mu\text{g m}^{-3}$ ) and minimum during monsoon ( $0.60 \pm 0.1 \mu\text{g m}^{-3}$ ), while the average OC concentration was  $12.4 \pm 5.3 \mu\text{g m}^{-3}$  with maximum loading during premonsoon ( $21.5 \pm 5.1 \mu\text{g m}^{-3}$ ) and minimum during the monsoon ( $1.5 \pm 1.1 \mu\text{g m}^{-3}$ ).

To estimate the SOC mass concentrations, we have used the EC tracer method as done by several others (Turpin and Huntzicker, 1995; Mukherjee et al., 2022). This method is based on measured OC and EC mass concentrations and the use of an appropriate primary OC-to-EC ratio:

$$POC \equiv [EC] \times \setminus (OC \setminus / EC \setminus) \quad (Pri) \quad (\text{Eq 7})$$

$$SOC \equiv [OC] - [PQC] \equiv [OC] - [EC] \times (OC / EC) \quad (\text{Pri}) \quad \text{(Eq 8)}$$

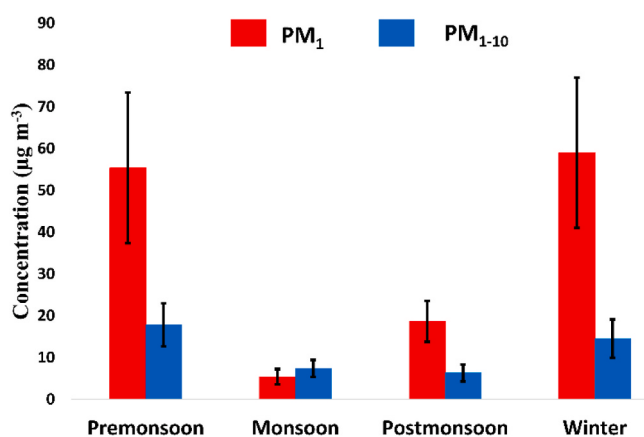


**Fig. 3.** Seasonal variability of (a) PM<sub>1</sub> and (b) PM<sub>1-10</sub> aerosols over Darjeeling

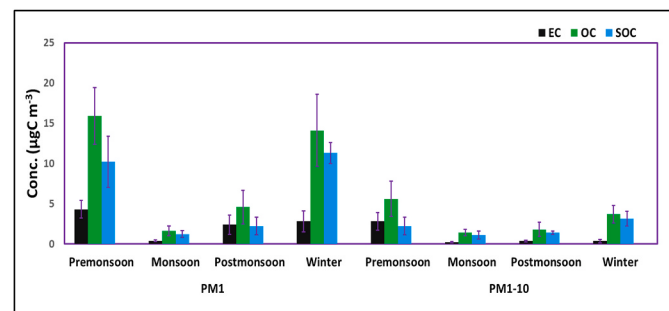


**Fig. 4.** Seasonal Variability of carbonaceous components of PM<sub>1</sub> and PM<sub>1-10</sub> over Darjeeling.

where the  $(OC/EC)_{pri}$  is the primary OC/EC ratio in freshly emitted combustion aerosols. The pivotal point of the EC tracer method is to judge the most preferable value of the  $(OC/EC)_{pri}$  ratio, which greatly varies with the geography, aerosol type, and sources and is highly sensitive to the method used for its estimation (Turpin and Huntzicker, 1995). Several groups have different approaches as reported in the literature for the estimation of  $(OC/EC)_{pri}$ , such as with the minimum OC/EC ratio or by using the lower percentiles of OC/EC, or through the minimum R-square method (MRS), etc. (Wu et al., 2019; Kaskaoutis et al., 2020). Recently, Wu et al. (2019) have fused the EC tracer approach with MRS and formulated a more robust method of estimating SOC compared to other methods. In the MRS method, it is assumed that the EC is always unrelated to SOC and, thus, the  $(OC/EC)_{pri}$  should be the ratio that provides in minimum association ( $\sim R^2$  almost near to zero) between the predicted SOC and measured EC (Wu et al., 2019; Kaskaoutis et al., 2020). In this study, we have individually predicted the SOC for the  $PM_{1}$  and  $PM_{1-10}$  for all the seasons using the aforementioned MRS method.

During premonsoon and winter, EC and OC (and SOC) showed higher loading in PM<sub>1</sub> (EC:  $4.3 \pm 1.1 \mu\text{g m}^{-3}$  in premonsoon and  $2.8 \pm 1.3 \mu\text{g m}^{-3}$  in winter; OC:  $15.9 \pm 3.5 \mu\text{g m}^{-3}$  premonsoon and  $14.1 \pm 2.1 \mu\text{g m}^{-3}$  in winter; SOC:  $10.2 \pm 3.2 \mu\text{g m}^{-3}$  in premonsoon and  $11.3 \pm 1.3 \mu\text{g m}^{-3}$  in winter) than PM<sub>1-10</sub> (EC:  $2.8 \pm 1.1 \mu\text{g m}^{-3}$  in premonsoon and  $0.36 \pm 0.2 \mu\text{g m}^{-3}$  in winter; OC:  $5.6 \pm 2.2 \mu\text{g m}^{-3}$  in premonsoon and  $3.7 \pm 1.1 \mu\text{g m}^{-3}$  in winter; SOC:  $2.2 \pm 1.1 \mu\text{g m}^{-3}$  in premonsoon and  $3.14 \pm 0.9 \mu\text{g m}^{-3}$  in winter).

#### 4.2. Long-term (2009–2021) trend of $PM_{1}$ , $PM_{1-10}$ , and $PM_{10}$

The time series analysis of the long-term annual PM<sub>10</sub> (Fig. 5a) reveals two-fold information. Firstly, a steady decrease in PM<sub>10</sub> ( $1.32 \mu\text{g m}^{-3} \text{ year}^{-1}$ ) was observed from 2009 to 2013. One of our recent studies (Sarkar et al., 2019) has also reported a decline in PM<sub>2.5</sub> during 2009–2013 because of an increase in mixing layer height leading to higher dispersion and the decreased fire spots over IGP and Nepal, the two most long-distant sources regions for eastern Himalaya.

Secondly, Fig. 5a also revealed a steep increase of PM<sub>10</sub> from 2014 to 2021 with a rate of 2.34  $\mu\text{g m}^{-3}$  year<sup>-1</sup>. In fact, in 2021, the annual concentration of PM<sub>10</sub> was only 3% less than the NAAQS level which is threatening for such an ecologically fragile region. In recent years, tourist arrival in the area has increased to about half a million every year (Das and Roy, 2016). This sharp increasing trend of PM<sub>10</sub> could be attributed to the massive increase in the tourism business along with uncontrolled over-urbanization over the years.

The trend of  $\text{PM}_1$  was similar to  $\text{PM}_{10}$  decreasing with a rate of  $1.8 \mu\text{g m}^{-3} \text{ year}^{-1}$  from 2009 to 2013 followed by a sharp increase with a rate of  $2.3 \mu\text{g m}^{-3} \text{ year}^{-1}$  during 2014–2021 (Fig. 5b). Although Darjeeling has yet not crossed the NAAQS value of  $\text{PM}_{10}$ , our results have revealed that the  $\text{PM}_1$  concentration alone has already crossed the NAAQS annual value of  $\text{PM}_{2.5}$  ( $40 \mu\text{g m}^{-3}$ ) since 2018 (Fig. 5b). Hence, in terms of  $\text{PM}_{2.5}$

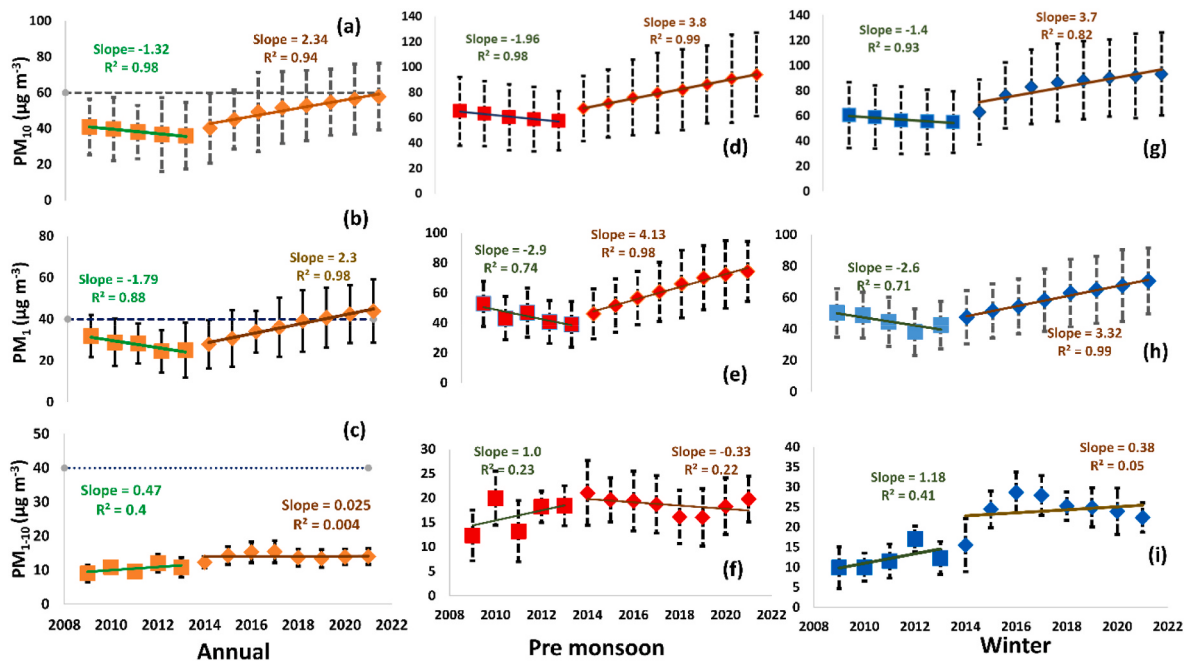


**Fig. 5.** Long-term (2009–2021) trends of annual (a–c), premonsoon (d–f), and winter (g–i) for PM<sub>10</sub> (upper panel), PM<sub>1</sub> (middle panel), and PM<sub>1–10</sub> (lower panel) over Darjeeling.

pollution, Darjeeling can be included in the list of “non-attainment” cities of India. In contrast, Fig. 5c shows that PM<sub>1–10</sub> has no significant trend during 2014–2021 and the concentration remains almost the same over the years. Fig. 5a and 5b has also revealed that the rate of increase of PM<sub>1</sub> and PM<sub>10</sub> is equal ( $2.3 \mu\text{g m}^{-3} \text{year}^{-1}$ ) for the period of 2014–2021. The regression analysis has also indicated a strong correlation between PM<sub>10</sub> and PM<sub>1</sub> ( $R^2 = 0.98$ ,  $P < 0.05$ ). The above results conclude that the increase of PM<sub>10</sub> greatly depends on and is influenced by PM<sub>1</sub> and not by the coarse mode particles, PM<sub>1–10</sub>. However, the decrease in PM<sub>10</sub> from 2009 to 2013 was associated with both PM<sub>1</sub> and PM<sub>1–10</sub> (Fig. 5a–c).

If we throw lights on the aerosol loading during premonsoon and winter, we can easily observe that in recent years the PM<sub>10</sub> pollution is comparable even with some urban atmospheres of the IGP. In-fact, PM<sub>10</sub> over Darjeeling can be compared with that over Kolkata metropolis in eastern India during the premonsoon (Ghosh et al., 2019). PM<sub>10</sub> exhibited a declining trend till 2013 during both seasons (premonsoon:  $2.0 \mu\text{g m}^{-3} \text{year}^{-1}$ ; winter:  $1.4 \mu\text{g m}^{-3} \text{year}^{-1}$ ). However, it further increased with the rate of  $3.8 \mu\text{g m}^{-3} \text{year}^{-1}$  in premonsoon and  $3.7 \mu\text{g m}^{-3} \text{year}^{-1}$  in winter. The high increasing rate of PM<sub>10</sub> could be attributed to the increase in local and regional anthropogenic emissions. To investigate the same, we have further studied the inter-annual variation of PM<sub>1</sub> as well as the rest part of PM<sub>10</sub> (PM<sub>1–10</sub>) for these two polluted seasons during 2009–2021 as shown in Fig. 5 e and f. When we look at the trend in PM<sub>1–10</sub> (Fig. 5f and 5i) no pattern was observed after 2013 during winter whereas before 2013, a steady increase was observed with a rate of  $1.2 \mu\text{g m}^{-3} \text{year}^{-1}$ . During premonsoon, a slow decreasing pattern ( $0.3 \mu\text{g m}^{-3} \text{year}^{-1}$ ) was found from 2014 to 2021 contrasting a slow and steady increasing trend from 2008 to 2013 ( $0.3 \mu\text{g m}^{-3} \text{year}^{-1}$ ). On the other hand, it can be observed from Fig. 5 (e and h), that PM<sub>1</sub> declined from 2008 to 2013 in both seasons with a rate of  $2.9 \mu\text{g m}^{-3} \text{year}^{-1}$  and  $2.6 \mu\text{g m}^{-3} \text{year}^{-1}$  respectively. However, the most interesting observation was the steep rise in PM<sub>1</sub> after 2013 ( $4.1 \mu\text{g m}^{-3} \text{year}^{-1}$  in premonsoon and  $3.3 \mu\text{g m}^{-3} \text{year}^{-1}$  in winter) as shown in Fig. 5e and 5h. Moreover, during 2018–2021, PM<sub>1</sub> was found to be as high as the PM<sub>10</sub> values of many plain land areas of the IGP.

The above findings, therefore, conclude that it is the PM<sub>1</sub> aerosol pollution during the premonsoon and winter seasons, which is

enhancing the annual PM<sub>10</sub> value and dragging it up near the NAAQS value. Therefore, we need to focus on these two seasons specifically for the PM<sub>1</sub> size regime to prevent the PM<sub>10</sub> pollution from exceeding the Indian standard.

#### 4.3. Future projection of aerosol pollution using autoregressive integrated moving average (ARIMA) model

We have attempted to investigate the future scenario of PM<sub>10</sub> and the influence of the high increasing trend of PM<sub>1</sub> on future PM<sub>10</sub> pollution. ARIMA model could be considered an important tool for the future projection of aerosols. Earlier studies have used this model for the prediction of aerosol optical depth (AOD) across the world (Li et al. 2019) though few in the Indian context (Taneja et al., 2016; Kumar et al., 2018; Nair et al., 2022; Dutta and Chatterjee, 2022). However, the use of this model with ground-based data in the prediction of aerosol loading in the future is the first-ever conducted in this study. We have shown the best-fit ARIMA model, output of ARIMA run, future projection, validation, and the p-value of the t-test for annual and seasonal PM<sub>10</sub> as well as for PM<sub>1</sub> during annual, winter, and premonsoon over Darjeeling. This has been illustrated in Fig. 6 (annual, premonsoon, and winter for PM<sub>1</sub> and PM<sub>10</sub>) and Fig S3 (a-b) (monsoon and postmonsoon, PM<sub>10</sub>). The residual analysis of the ARIMA model has been shown in Fig S2 (a-f) and S(3c) and S(3d). We have performed the model-based future prediction of aerosols from 2022 up to the year 2024. This prediction is based on a business-as-usual (BAU) scenario i.e. if the current sources and scenario remain the same and no further actions are taken to curb the aerosol pollution, then what would be the PM<sub>1</sub> and PM<sub>10</sub> scenario in 2024. Projected PM<sub>1</sub> and PM<sub>10</sub>, lower and upper confidence limits, best fit ARIMA model along with AIC and BIC values individually for seasons and annual in 2024 were computed and shown in Table 1.

We tested the performance of the model and the period of 2020–2021 was chosen as the validation period. We used the root mean square error (RMSE) and mean absolute error (MAE) for testing the performance of the model. RMSE and MAE during the model-observation validation period have been shown in Table S2 respectively. The small MAE (0.25 in premonsoon, 0.70 in winter, and 0.19 in annual for PM<sub>10</sub>; 4.42 in premonsoon, 0.31 in winter, and 0.12 in

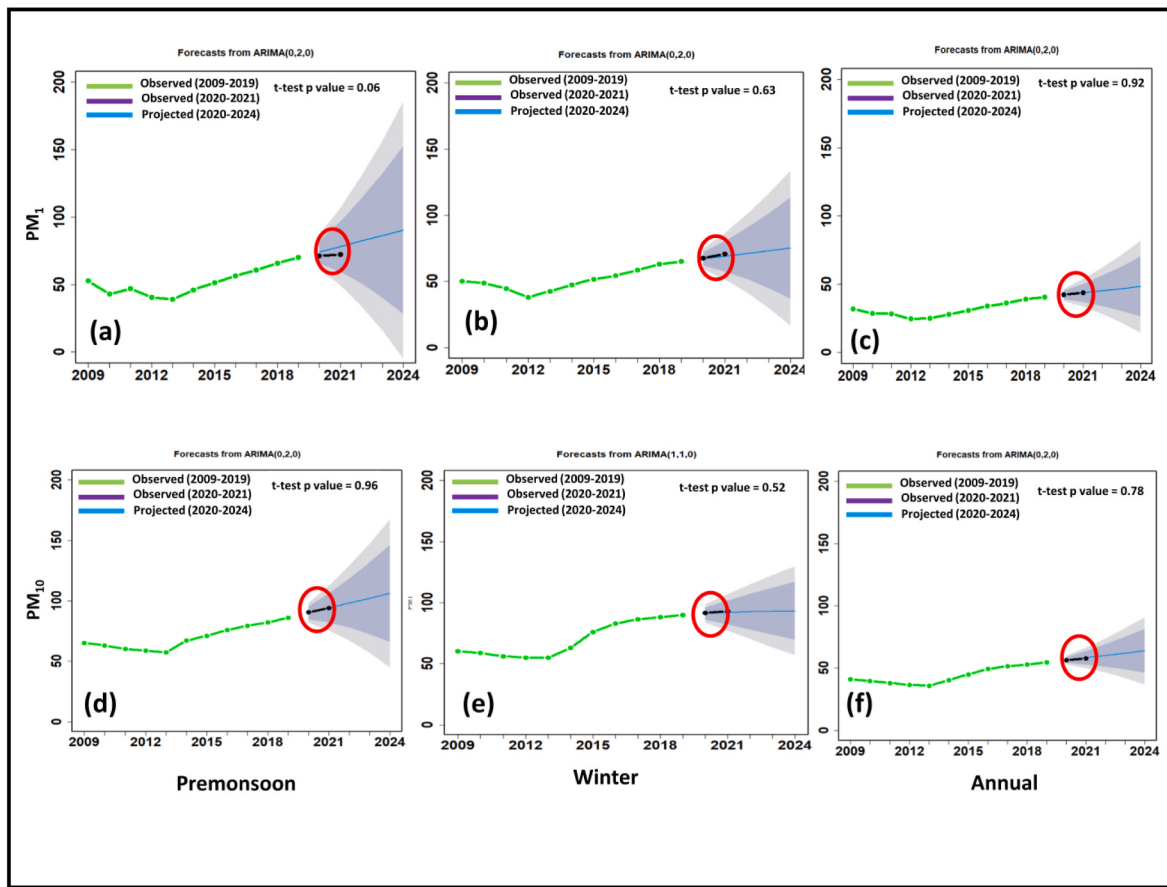


**Fig. 6.** Observed data for ARIMA model development (green line; 2009–2019), observed data for validation with ARIMA predicted values (black and blue lines within encircled areas; 2020–2021) and future prediction by ARIMA till 2024 (blue lines only) over Darjeeling in (a) premonsoon (PM<sub>1</sub>), (b) winter (PM<sub>1</sub>), (c) annual (PM<sub>1</sub>) (d) premonsoon (PM<sub>10</sub>), (e) winter (PM<sub>10</sub>) and (f) annual (PM<sub>10</sub>). Grey lines represent 95% upper and lower confidence limits.

**Table 1**

Projected PM<sub>10</sub> and PM<sub>1</sub> (using ARIMA) in 2024, the 95% confidence limit (for both lower (LL) and upper limit (UL)), best fit ARIMA model along with AIC and BIC values.

Size of aerosol	Seasons/Annual	PM ( $\mu\text{g}/\text{m}^3$ ) in 2024 (modelled)	Confidence Limit (95% LL)	Confidence Limit (95% UL)	The best fit ARIMA model	AIC/BIC value of the best-fit model
PM <sub>10</sub>	Annual	62.2	36.8	90.9	(0,2,0)	38.7/38.9
	Premonsoon	106.2	44.9	167.4	(0,2,0)	53.4/53.6
	Monsoon	13.1	10.7	15.5	(1,0,0)	33.7/34.9
	Post monsoon	34.3	18.1	52.5	(0,2,0)	30.5/30.7
	Winter	93.3	57.0	129.5	(1,1,0)	59.0/59.6
PM <sub>1</sub>	Annual	48.4	14.7	81.0	(0,2,0)	42.6/42.8
	Premonsoon	90.5	0.1	185.8	(0,2,0)	61.4/61.6
	Winter	75.2	16.7	133.7	(0,2,0)	52.6/52.8

**Table 2**

PM<sub>10</sub> and PM<sub>1</sub> in 2019 (observation) and 2024 (modelled using ARIMA) and their percentage change from 2019 to 2024.

Size	Seasons/Annual	PM ( $\mu\text{g}/\text{m}^3$ ) in 2019 (observed)	PM ( $\mu\text{g}/\text{m}^3$ ) in 2024 (modelled)	Percentage Change from 2019 to 2024
PM <sub>10</sub>	Annual	54.2	62.2	15.8
	Premonsoon	86.1	106.2	23.2
	Monsoon	13.3	13.1	-1.6
	Post monsoon	30.8	34.3	11.3
	Winter	86.1	95.3	10.7
PM <sub>1</sub>	Annual	40.7	48.4	21.0
	Premonsoon	70.0	90.5	29.1
	Winter	64.9	75.2	15.8

annual; PM<sub>1</sub>) and RMSE (0.32 in premonsoon, 0.76 in winter, 0.21 in annual for PM<sub>10</sub>; 4.7 in premonsoon, 0.36 in winter and 0.14 in annual; PM<sub>1</sub>) values indicate that the model performed exceptionally well. The p-value of the t-test (illustrated in Fig. 6) exhibits values greater than 0.05 indicating significant similarities between model prediction and observation and therefore the model performance was excellent.

The PM<sub>1</sub> and PM<sub>10</sub> loadings during premonsoon and winter in 2019, the predicted loadings in 2024, and the percentage changes in 2024 concerning 2019 have been shown in Table 2. The model revealed that under the BAU scenario, Darjeeling would experience PM<sub>10</sub> loading of  $62.2 \mu\text{g}/\text{m}^3$  exceeding the annual NAAQS ( $60 \mu\text{g}/\text{m}^3$ ) by  $\sim 16\%$  in 2024 and would be included in the list of non-attainment cities. From Tables 2 and it is clear that the exceedance of the annual average of PM<sub>10</sub> over the Indian standard would mainly be fostered by its loadings in premonsoon ( $106.1 \mu\text{g}/\text{m}^3$  with an increase of 23.2% compared to 2019) and winter

( $95.3 \mu\text{gm}^{-3}$  with the increase of 10.7% compared to 2019). Even with the increase of 11.3%,  $\text{PM}_{10}$  during postmonsoon would be around  $34 \mu\text{gm}^{-3}$ . In contrast, future projection during monsoon shows a decline of 1.6% of  $\text{PM}_{10}$  in 2024 compared to 2019. The model also revealed that  $\text{PM}_1$  would reach  $90.5 \mu\text{gm}^{-3}$  (29% increase from 2019) and  $75.2 \mu\text{gm}^{-3}$  (16% increase from 2019) during premonsoon and winter respectively in the year 2024. The most important feature of the future prediction with serious concern is that the concentration of  $\text{PM}_1$  ( $48.4 \mu\text{gm}^{-3}$ ) would exceed the annual average of NAAQS of  $\text{PM}_{2.5}$  ( $40 \mu\text{gm}^{-3}$ ) by 21% in 2024. The  $\text{PM}_{10}$  pollution scenario over this eastern Himalayan high-altitude station in 2024 would be similar to that over several Indian metro-cities and the most polluted IGP regions. It would not be an overstatement if we say that the  $\text{PM}_1$  pollution over Darjeeling would be comparable with the  $\text{PM}_{2.5}$  pollution over Indian metro-cities and several plain-land urban regions and would have no comparison with other high-altitude stations probably across the world.

The results coming out of the model-based future prediction is indeed uncomfortable and of serious concern and draws attention to the policy makers.

Therefore, our study at this point needed an in-depth knowledge of the major sources and regional/long-distant source regions of  $\text{PM}_1$  that enhanced the cumulative  $\text{PM}_{10}$  pollution as well as would be responsible for high pollution in the future if not controlled. This has been discussed below.

#### 4.4. Source apportionment of $\text{PM}_1$ aerosols by PMF model and identification of major source regions by CWT analysis

PMF provides the normalized contribution of all the factors to the total mass in such a way that allows for a comparison of the temporal pattern of source contributions. Hence from the model obtained temporally resolved factor contributions, we have estimated the mean contribution of different factors for the  $\text{PM}_1$  aerosols during premonsoon and winter. The optimal solution for the model was obtained for five factors. The data screening method and optimizing conditions have already been discussed in the methodology section. The statistical parameters are given in the supplementary section in Table S1. While observing the time series of  $\text{PM}_1$ , we observed a slow decrease from 2009 to 2013 followed by a steady increase from 2014 to 2021. Thus, assuming a major increase in the local source profile over the sampling station we have apportioned the sources of  $\text{PM}_1$  from 2014 onwards. The total number of samples used in the model run was 186 (90 in winter and 96 in premonsoon).

The species fingerprints along with the relative contribution of each

factor are depicted in Figs. 7 and 8 and discussed below.

**Factor 1:** The first factor could be associated with the polluted dust (dust mixed with smoke) as it is loaded heavily with  $\text{Ca}^{2+}$ ,  $\text{Mg}^{2+}$ , and  $\text{Na}^+$  and moderately with EC, OC,  $\text{NO}_3^-$  and  $\text{SO}_4^{2-}$  (Jordan et al., 2003; Chatterjee et al., 2010; Ghosh et al., 2021). CWT analysis (Fig. 9) reveals the transport of air masses originating from the IGP and the arid/semi-arid regions of western India. These air masses could bring ultrafine dust particles well mixed with several anthropogenic pollutants (from fossil fuel and biomass burning) while passing over IGP. Such dust transport mixed with other polluted components has been found to be prominent during premonsoon. As shown in Fig. S1, the thick layer of polluted dust aerosols over Darjeeling as observed from CALIPSO strengthens the fact well. This factor contributes nearly 15% during the premonsoon and 8% during the winter to the total  $\text{PM}_1$ .

**Factor 2:** Factor 2 well represents coal burning as the factor has high loading of OC,  $\text{Cl}^-$  and  $\text{SO}_4^{2-}$ , and moderate loading of EC and  $\text{K}^+$  (Hailin et al., 2008; Chatterjee et al., 2010; Yu et al., 2018; Pan et al., 2018). In addition to the over-abundance of tourist vehicles, the coal combustion from the Darjeeling Himalayan Railway (a UNESCO world heritage narrow gauge railway that still runs on coal) that runs in higher frequency in premonsoon and winter seasons could be one of the major contributors. The use of coal in several hotels, resorts as well as road-side eateries is very common in Darjeeling. While this factor contributes 20% to the total  $\text{PM}_1$  load during winter, contributes only 10% during the premonsoon.

**Factor 3:** The high abundances of  $\text{K}^+$ , EC, OC,  $\text{SO}_4^{2-}$  along with moderate  $\text{NH}_4^+$  and  $\text{Cl}^-$  in this factor strongly suggest the biomass burning emissions (Jain and Sharma, 2020; Xiao et al., 2020; Zhou et al., 2021). CWT analysis (Fig. 9) reveals that the carbonaceous and secondary water-soluble components of  $\text{PM}_1$  are more local or regional. This well indicates that regional or local biomass burning is an important source of  $\text{PM}_1$  over the eastern Himalayas both in premonsoon and winter. The high influx of tourists and the associated biomass-burning activities over Darjeeling during premonsoon have been well established (Chatterjee et al., 2012; Sharma et al. 2020; Chatterjee et al., 2020; Ghosh et al., 2021; Sharma et al. 2021; Mukherjee et al., 2022). However, the influence of crop residue burning over the western IGP could not be ruled out too. The presence of elevated smoke over Darjeeling (Fig. S1) as retrieved from CALIPSO, well synchronizes with the source apportionment and CWT analysis (Fig. 9) and hence strengthens the fact. In contrast, biomass burning is a common and frequent practice in Darjeeling during winter to combat the chilly cold weather (Roy et al., 2017). The CALIPSO observation also identified continental smoke over the sampling site during winter (Fig. S1). However, the transport of

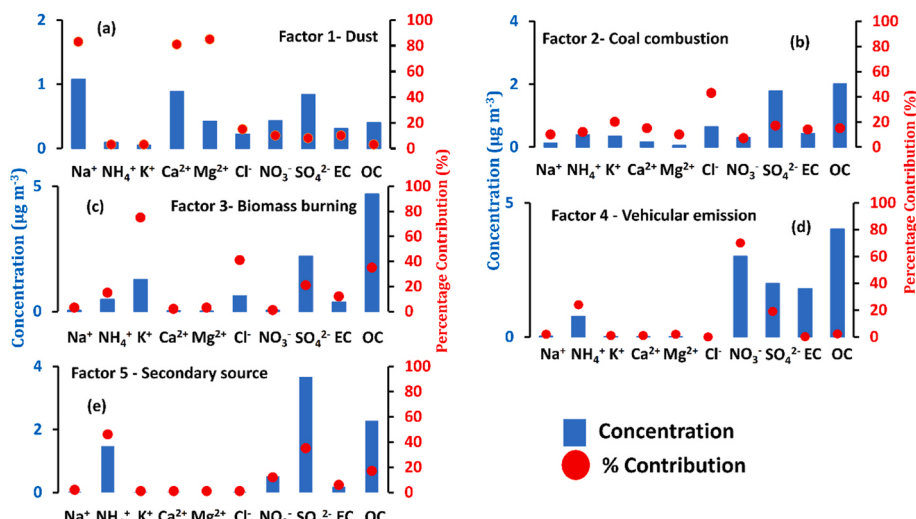


Fig. 7. The factor finger printing of different sources of  $\text{PM}_1$  aerosols over Darjeeling.

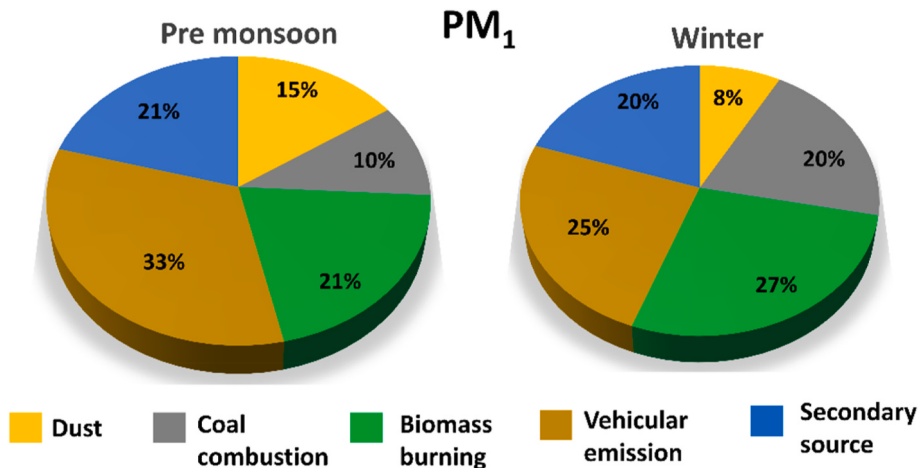


Fig. 8. Contribution of different sources to PM<sub>1</sub> aerosols over Darjeeling during premonsoon and winter.

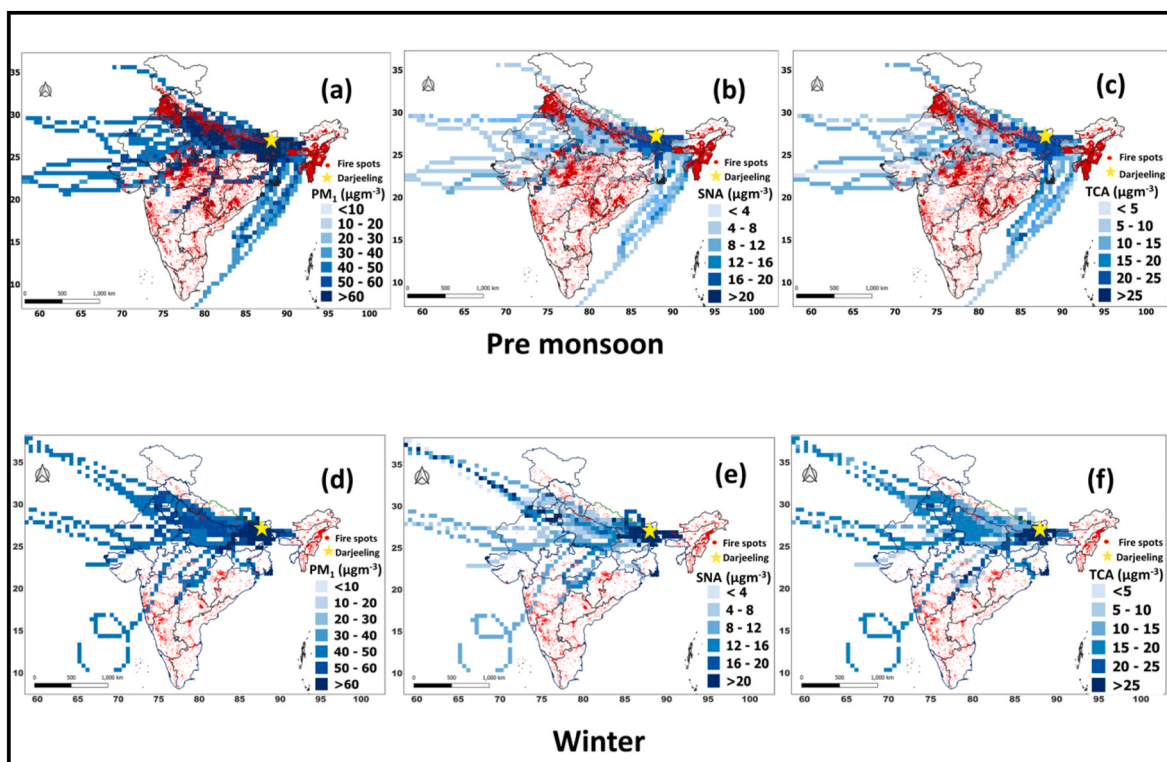


Fig. 9. Concentration weighted trajectories of the PM<sub>1</sub> (left panel) and its secondary inorganic (middle panel) and carbonaceous components (right panel) during premonsoon and winter over Darjeeling.

ultrafine biomass-burning aerosols from IGP could also contribute significantly because of the common practice of biomass burning along the entire IGP regions mainly over the rural regions. While the factor contributes 27% of the PM<sub>1</sub> during the winter, the contribution during the premonsoon was nearly 21%.

**Factor 4:** The fourth factor could be easily associated with vehicular emissions because of the high loadings of NO<sub>3</sub><sup>-</sup>, OC, and EC with the moderate loading of NH<sub>4</sub><sup>+</sup> and SO<sub>4</sub><sup>2-</sup>. During premonsoon, as stated earlier, Darjeeling experiences enormous tourist-related vehicular activities (Chatterjee et al., 2010, 2012; Roy et al., 2017; Ghosh et al., 2021) as well as the use of diesel-driven power generators in several hotels, and resorts, etc as the power cut is a frequent occurrence during this season in Darjeeling. On the other hand, during winter, local vehicular emission remains constant. The most important and notable

feature is that this factor alone contributes 33% and 25% to the total PM<sub>1</sub> load in premonsoon and winter respectively.

**Factor 5:** Factor 5 is consisting of secondary inorganic species NH<sub>4</sub><sup>+</sup>, SO<sub>4</sub><sup>2-</sup>, OC, and moderate NO<sub>3</sub><sup>-</sup>. In one of our recent studies (Ghosh et al., 2021), we observed aqueous phase oxidation of SO<sub>2</sub> and the formation of (NH<sub>4</sub>)<sub>2</sub>SO<sub>4</sub> under NH<sub>3</sub> rich conditions (Ghosh et al., 2020) over Darjeeling. In a study over Svalbard Archipelago, Yu et al. (2019) found that 74% of non-sea-salt sulfate particles were coated with organic matter whereas 20% of sulfate particles had soot inclusions which only appeared in the organic matter coating. In Bakersfield, California, carbonaceous aerosols were found to be internally mixed with ammonium and sulfate from the partitioning of ammonium sulfate (Whiteaker et al., 2002). These inorganic secondary components were found to be more regional (Fig. 9) and could get mixed with the local carbonaceous

components. Therefore, this factor could be assigned to the secondary inorganic aerosols coated with carbons (Chatterjee et al., 2021). This factor almost equally contributes (20–21%) to PM<sub>1</sub> during premonsoon and winter.

#### 4.4.1. Most influencing sources of PM<sub>1</sub> for high PM<sub>10</sub> pollution

To understand the most influential source of PM<sub>1</sub> responsible for high PM<sub>10</sub> pollution, we have conducted the source apportionment of PM<sub>10</sub> using PMF for the two polluted seasons; premonsoon and winter. Similar to PM<sub>1</sub>, the PMF model gives a 5-factor optimal solution for PM<sub>10</sub>. The comparison of source contributions for both PM<sub>1</sub> and PM<sub>10</sub> during premonsoon and winter has been shown in Fig. S5. Results have revealed that for both the PM<sub>1</sub> and PM<sub>10</sub>, vehicular emission (33% and 28% respectively) was the most dominating and influencing source followed by biomass burning (21%), secondary aerosol (21% and 20% respectively), dust (15% and 18% respectively) and coal burning (10% and 13% respectively) in premonsoon season. On the other hand, during winter, biomass burning (27% and 23% respectively) was the most contributing source followed by vehicular emission (25% and 24% respectively). The other factors follow the same order of contribution (coal burning: 20% in PM<sub>1</sub> and 23% in PM<sub>10</sub>; secondary aerosol: 20% in both; dust: 8% in PM<sub>1</sub> and 10% in PM<sub>10</sub>). The percentage contribution of a given source of PM<sub>1</sub> to that in PM<sub>10</sub> has been calculated and shown in Fig. S6. Results are indicating that any given source in PM<sub>1</sub> contributed to that particular source in PM<sub>10</sub> by 60–90%. The most important outcome is that the contribution of vehicular emissions to PM<sub>1</sub> is >90% of that to PM<sub>10</sub> in premonsoon whereas the contribution of biomass burning to PM<sub>1</sub> is >80% of that to PM<sub>10</sub> in winter. Therefore, vehicular emissions in premonsoon and biomass burning in winter are the two most influencing sources that need to be controlled and curbed to mitigate PM<sub>1</sub> and hence PM<sub>10</sub> pollution over Darjeeling.

## 5. Summary

The present study was conducted on PM<sub>10</sub> pollution and its major causes and sources over a long-term period (2009–2021) as well as its future projection over a high-altitude urban atmosphere in the eastern Himalayas in India. The major findings of the study could be summarized as follows:

- The long-term (2009–2021) average concentration of PM<sub>10</sub> was  $46 \pm 8 \mu\text{g m}^{-3}$  and none of the years of the study period showed exceedance of PM<sub>10</sub> loading over NAAQS ( $60 \mu\text{g m}^{-3}$ ). However, distinct seasonal variability revealed the highest PM<sub>10</sub> pollution during winter ( $74.0 \pm 15.1 \mu\text{g m}^{-3}$ ) and premonsoon ( $73.1 \pm 12.1 \mu\text{g m}^{-3}$ ).
- Bi-modal distribution pattern of aerosol was observed for all the seasons with a larger peak at the fine mode. Secondary inorganic aerosols and organic carbon were the most abundant components of the aerosols and were mostly confined within the fine mode.
- The long-term trend has revealed that despite the PM<sub>10</sub> value never exceeding the NAAQS value yet the annual PM<sub>1</sub> concentration already exceeded the NAAQS PM<sub>2.5</sub> ( $40 \mu\text{g m}^{-3}$ ) value since 2018.
- The inter-annual variability of PM<sub>10</sub> exhibited a steady decrease during 2009–2013 at the rate of  $2.0 \mu\text{g m}^{-3} \text{ yr}^{-1}$  in premonsoon and  $1.4 \mu\text{g m}^{-3} \text{ yr}^{-1}$  in winter. Since 2014, a sharp rise in PM<sub>10</sub> was observed at the rate of  $3.8 \mu\text{g m}^{-3} \text{ yr}^{-1}$  in premonsoon and  $3.7 \mu\text{g m}^{-3} \text{ yr}^{-1}$  in winter.
- We observed that the key factor responsible for high PM<sub>10</sub> pollution in premonsoon and winter is the ultrafine fraction of PM<sub>10</sub> i.e. PM<sub>1</sub>. PM<sub>1</sub> was found to rise sharply at a rate of  $4.1 \mu\text{g m}^{-3} \text{ yr}^{-1}$  in premonsoon and  $3.3 \mu\text{g m}^{-3} \text{ yr}^{-1}$  in winter since 2014. On the other hand, PM<sub>10</sub> did not show any remarkable changes since 2014 compared to PM<sub>1</sub>.
- The ARIMA model projects PM<sub>1</sub> to be  $90.5 \mu\text{g m}^{-3}$  in premonsoon and  $75.2 \mu\text{g m}^{-3}$  in winter in the year 2024. The most important and

alarming outcome of the ARIMA model is that the PM<sub>10</sub> pollution would reach and exceed its NAAQS in 2024 under a business-as-usual scenario. The model predicts that the annual average concentration of PM<sub>10</sub> and PM<sub>1</sub> in 2024 would be  $62.2 \mu\text{g m}^{-3}$  and  $48.4 \mu\text{g m}^{-3}$  respectively and cross the respective NAAQS of PM<sub>10</sub> and PM<sub>2.5</sub>. It would therefore be included as one of the non-attainment cities of India concerning PM<sub>10</sub> as well as PM<sub>2.5</sub> pollution.

- Source apportionment of PM<sub>1</sub> using the PMF model revealed five major sources both in premonsoon and winter. During premonsoon, the major dominating source was vehicular emissions (33%) followed by biomass burning and secondary inorganic aerosols (each of 21%), polluted dust (15%), and coal burning (10%). During winter the major sources were biomass burning (27%) and vehicular emission (25%). The contribution of coal burning was more (20%) whereas polluted dust was less (8%) in winter. Interestingly, the contribution of secondary inorganic aerosols in winter remained almost equal to that of premonsoon (20%).
- Vehicular emissions in PM<sub>1</sub> contributed >90% of PM<sub>10</sub> in premonsoon and biomass burning in PM<sub>1</sub> contributed >80% in winter therefore, these two sources need to be controlled to mitigate PM<sub>1</sub> and hence PM<sub>10</sub> pollution over this part of eastern Himalaya.

## 6. Conclusion and implication of the study

The high PM<sub>10</sub> pollution over a high-altitude urban atmosphere in the eastern Himalayas is mainly due to high premonsoon and winter-time PM<sub>1</sub> pollution i.e. the ultrafine fraction of PM<sub>10</sub>. Source apportionment study revealed that 80–85% of PM<sub>1</sub> pollution was due to local/regional anthropogenic activities, specifically combustion activities. These anthropogenic activities are mainly related to uncontrolled tourist influx, unplanned over-urbanization, lack of surveillance on unauthorized land-use, biomass, and other combustion activities, use of old vehicles, diesel-driven generator sets, etc. Though the premonsoon and winter-time PM<sub>1</sub> pollution has been high enough in recent years, the PM<sub>10</sub> loading remained within the NAAQS. However, if proper and stringent actions are not taken seriously, this high-altitude urban atmosphere in the eastern Himalayas would become a “non-attainment” city soon (2024). The most alarming feature is that PM<sub>1</sub> loading in winter and premonsoon would be comparable with PM<sub>2.5</sub> loading over several plain-land metropolis and urban atmospheres.

The national mission of the Govt. of India, the National Clean Air Program (NCAP) is addressing 131 polluted cities across the country for the mitigation of air pollutants, especially aerosols, PM<sub>2.5</sub>, and PM<sub>10</sub>. But several regions with polluted urban atmospheres remained unexplored and hence excluded from this national mission. The present study throws light on one of the geographically, climatically, and ecologically important high-altitude Himalayan stations in India where people have been contributing as well as experiencing huge pollution load but remained out of sight of the policy makers. The study raises a serious concern in front of the policy makers that a high-altitude tourist station like Darjeeling in the eastern Himalayas would soon become a non-attainment city. Therefore, central and state pollution control boards need to think of building various robust and continuous monitoring stations for air pollutants in such regions immediately. It would help build a good database for better understanding the aerosol pollution scenario for such un-noticed but important parts of the country under the umbrella of NCAP in near future. Another important aspect of the study is hitting the exact size (and its sources) that enhances the load of composite aerosols. We are building the policies and action plans for mitigating PM<sub>2.5</sub> or PM<sub>10</sub> by making the source apportionment of those composite aerosols. But such source apportionment could be inefficient for providing correct features of truly responsible sources that need to be mitigated. Therefore, the present study emerges as an example of the appropriate approach for aerosol pollution control, first by identifying the exact size of aerosol hikes and then its sources. It would then ease the efforts as well as financial investments towards mitigation programs

than doing the same for composite aerosols.

## CRediT authorship contribution statement

**Abhinandan Ghosh:** Planning, Investigation, Data curation, Formal analysis, Chemical analysis, Formal analysis, figures, Writing – original draft, and, Writing – review & editing, review. **Monami Dutta:** Investigation, Data curation, Formal analysis, figures, manuscript preparation, Writing – review & editing, writing review, and formatting the manuscript. **Abhijit Chatterjee:** Conceptualization, Concept, Investigation, Data curation, Writing – original draft, and, Writing – review & editing, review, Funding acquisition, fund accusation, and overall, Supervision.

## Declaration of competing interest

We hereby declare that we have no known competing financial interests or personal relationships that could have appeared to influence the work reported in this paper.

## Data availability

Data will be made available on request.

## Acknowledgment

The authors would like to thank the Science and Engineering Research Board, Department of Science and Technology, Government of India for financially supporting the study under IRHPA (Intensification of Research in High Priority Areas/Sanction No. IR/S2/PF.01/2011) scheme. Thanks are due to Mr. Sabyasachi Majhee and Mrs. Debolina Seal for their technical support. Thanks, are also due to Dr. Anandamay Adak, Mrs. Yasadhara Yadav, and Mr. Deo Kumar Rai for their logistic support.

## Appendix A. Supplementary data

Supplementary data to this article can be found online at <https://doi.org/10.1016/j.atmosenv.2023.119845>.

## References

- Adak, A., Chatterjee, A., Singh, A.K., Sarkar, C., Ghosh, S., Raha, S., 2014. Atmospheric fine mode particulates at eastern Himalaya, India: role of meteorology, long-range transport and local anthropogenic sources. *Aerosol Air Qual. Res.* 14 (1), 440–450.
- Andreae, M.O., 1983. Soot carbon and excess fine potassium: long-range transport of combustion-derived aerosols. *Science* 220 (4602), 1148–1151.
- Bouwman, A.F., Lee, D.S., Asman, W.A., Dentener, F.J., Van Der Hoek, K.W., Olivier, J.G. J., 1997. A global high-resolution emission inventory for ammonia. *Global Biogeochem. Cycles* 11 (4), 561–587.
- Box, G.E.P., Jenkins, G.M., 1976. *Times Series Analysis-Forecasting and Control*. Prentice-Hall, Englewood Cliffs.
- Box, G.E.P., Jenkins, G.M., Reinsel, G.C., 1994. *Time Series Analysis: Forecasting and Control*, third ed. Prentice Hall, Englewood Cliffs.
- Cesari, D., Amato, F., Pandolfi, M., Alastuey, A., Querol, X., Contini, D., 2016a. An inter-comparison of PM10 source apportionment using PCA and PMF receptor models in three European sites. *Environ. Sci. Pollut. Control Ser.* 23 (15), 15133–15148.
- Cesari, D., Donato, A., Conte, M., Contini, D., 2016b. Inter-comparison of source apportionment of PM10 using PMF and CMB in three sites nearby an industrial area in central Italy. *Atmos. Res.* 182, 282–293.
- Cesari, D., Merico, E., Dinoi, A., Marinoni, A., Bonasoni, P., Contini, D., 2018. Seasonal Variability of Carbonaceous Aerosols in an Urban Background Area in Southern Italy, vol. 200. *Atmospheric Research*, pp. 97–108.
- Chatterjee, A., Adak, A., Singh, A.K., Srivastava, M.K., Ghosh, S.K., Tiwari, S., Devara, P. C., Raha, S., 2010. Aerosol chemistry over a high altitude station at northeastern Himalayas, India. *PLoS One* 5 (6), e11122.
- Chatterjee, A., Ghosh, S.K., Adak, A., Singh, A.K., Devara, P.C., Raha, S., 2012a. Effect of dust and anthropogenic aerosols on columnar aerosol optical properties over Darjeeling (2200 m asl), eastern Himalayas, India. *PLoS One* 7 (7), e40286.
- Chatterjee, A., Dutta, C., Jana, T.K., Sen, S., 2012b. Fine mode aerosol chemistry over a tropical urban atmosphere: characterization of ionic and carbonaceous species. *J. Atmos. Chem.* 69, 83–100.
- Chatterjee, A., Dutta, M., Ghosh, A., Ghosh, S.K., Roy, A., 2020. Relative role of black carbon and sea-salt aerosols as cloud condensation nuclei over a high altitude urban atmosphere in eastern Himalaya. *Sci. Total Environ.* 742, 140468.
- Chatterjee, A., Mukherjee, S., Dutta, M., Ghosh, A., Ghosh, S.K., Roy, A., 2021. High rise in carbonaceous aerosols under very low anthropogenic emissions over eastern Himalaya, India: impact of lockdown for COVID-19 outbreak. *Atmos. Environ.* 244, 117947.
- Chow, J.C., Watson, J.G., Chen, L.W.A., Arnott, W.P., Moosmüller, H., Fung, K., 2004. Equivalence of elemental carbon by thermal/optical reflectance and transmittance with different temperature protocols. *Environ. Sci. Technol.* 38 (16), 4414–4422.
- Das, R., Roy, K., 2016. Tracing the concept of alternative tourism for the preservation of the ethnic socio-cultural life and environment in Darjeeling Hills. *Indian J. Adv. Res. Innov. Ideas Educ.* 2 (6).
- Draxler, R., Stunder, B., Rolph, G., Stein, A., Taylor, A., 2016. HySplit user's guide. [https://www.arl.noaa.gov/documents/reports/hysplit\\_user\\_guide.pdf](https://www.arl.noaa.gov/documents/reports/hysplit_user_guide.pdf).
- Duan, F., Liu, X., Yu, T., Cachier, H., 2004. Identification and estimate of biomass burning contribution to the urban aerosol organic carbon concentrations in Beijing. *Atmos. Environ.* 38 (9), 1275–1282.
- Dutta, M., Chatterjee, A., 2022. A deep insight into state-level aerosol pollution in India: long-term (2005–2019) characteristics, source apportionment, and future projection. *Atmos. Environ.* 289, 119312, 2023.
- Dutta, M., Ghosh, A., Sharma, S.K., Mandal, T.K., Chatterjee, A., 2023. CCN Activation of Ultrafine Biogenic-WSOC under Restricted Anthropogenic Emissions: A Study over Eastern Himalaya in India. *Atmospheric Research*, 106704.
- Gadi, R., Sharma, S.K., Mandal, T.K., 2019. Source apportionment and health risk assessment of organic constituents in fine ambient aerosols (PM<sub>2.5</sub>): a complete year study over National Capital Region of India. *Chemosphere* 221, 583–596.
- Ghosh, A., Roy, A., Chatterjee, A., Das, S.K., Ghosh, S.K., Raha, S., 2019. Impact of biomass burning plumes on the size-segregated aerosol chemistry over an urban atmosphere at Indo-Gangetic Plain. *Aerosol Air Qual. Res.* 19 (1), 163–180.
- Ghosh, A., Roy, A., Das, S.K., Ghosh, S.K., Raha, S., Chatterjee, A., 2020. Identification of most preferable reaction pathways for chloride depletion from size segregated sea-salt aerosols: a study over high altitude Himalaya, tropical urban metropolis and tropical coastal mangrove forest in eastern India. *Chemosphere* 245, 125673.
- Ghosh, A., Patel, A., Rastogi, N., Sharma, S.K., Mandal, T.K., Chatterjee, A., 2021. Size-segregated aerosols over a high altitude Himalayan and a tropical urban metropolis in Eastern India: chemical characterization, light absorption, role of meteorology and long range transport. *Atmos. Environ.* 254, 118398.
- Gupta, I., Salunkhe, A., Kumar, R., 2012. Source Apportionment of PM10 by Positive Matrix Factorization in Urban Area of Mumbai, India. *The Scientific World Journal*, 2012.
- Hailin, W., Zhuang, Y., Ying, W., Yele, S.U.N., Hui, Y.U.A.N., Zhuang, G., Zhengping, H. A.O., 2008. Long-term monitoring and source apportionment of PM<sub>2.5</sub>/PM10 in Beijing, China. *J. Environ. Sci.* 20 (11), 1323–1327.
- Hsu, Y.K., Holsen, T.M., Hopke, P.K., 2003. Comparison of hybrid receptor models to locate PCB sources in Chicago. *Atmos. Environ.* 37 (4), 545–562.
- Jain, S., Sharma, T., 2020. Social and travel lockdown impact considering coronavirus disease (COVID-19) on air quality in megacities of India: present benefits, future challenges and way forward. *Aerosol Air Qual. Res.* 20 (6), 1222–1236.
- Jain, S., Sharma, S.K., Choudhary, N., Masiwal, R., Saxena, M., Sharma, A., Mandal, T.K., Gupta, A., Gupta, N.C., Sharma, C., 2017. Chemical characteristics and source apportionment of PM<sub>2.5</sub> using PCA/APCS, UNMIX, and PMF at an urban site of Delhi, India. *Environ. Sci. Pollut. Control Ser.* 24 (17), 14637–14656.
- Jiang, W., Wang, Y., Tsou, M.H., Fu, X., 2015. Using social media to detect outdoor air pollution and monitor air quality index (AQI): a geo-targeted spatiotemporal analysis framework with Sina Weibo (Chinese Twitter). *PLoS One* 10 (10), e0141185.
- Jordan, C.E., Dibb, J.E., Anderson, B.E., Fuelberg, H.E., 2003. Uptake of nitrate and sulfate on dust aerosols during TRACE-P. *J. Geophys. Res. Atmos.* 108 (D21).
- Karar, K., Gupta, A.K., 2006. Seasonal variations and chemical characterization of ambient PM10 at residential and industrial sites of an urban region of Kolkata (Calcutta), India. *Atmos. Res.* 81 (1), 36–53.
- Kaskaoutis, D.G., Grivas, G., Theodosi, C., Tsagkaraki, M., Paraskevopoulou, D., Stavroulas, I., Liakakou, E., Gkikas, A., Hatzianastassiou, N., Wu, C., Gerasopoulos, E., 2020. Carbonaceous aerosols in contrasting atmospheric environments in Greek cities: evaluation of the EC-tracer methods for secondary organic carbon estimation. *Atmosphere* 11 (2), 161.
- Kumar, A., Sarin, M.M., 2010. Atmospheric water-soluble constituents in fine and coarse mode aerosols from high-altitude site in western India: long-range transport and seasonal variability. *Atmos. Environ.* 44 (10), 1245–1254.
- Kumar, M., Parmar, K.S., Kumar, D.B., Mhawish, A., Broday, D.M., Mall, R.K., Banerjee, T., 2018. Long-term aerosol climatology over Indo-Gangetic Plain: trend, prediction and potential source fields. *Atmos. Environ.* 180, 37–50.
- Li, W., Shao, L., 2009. Transmission electron microscopy study of aerosol particles from the brown hazes in northern China. *J. Geophys. Res. Atmos.* 114 (D9).
- Li, X., Zhang, C., Zhang, B., Liu, K., 2019. A comparative time series analysis and modeling of aerosols in the contiguous United States and China. *Sci. Total Environ.* 690, 799–811.
- Massey, D.D., Habil, M., Taneja, A., 2016. Particles in different indoor microenvironments-its implications on occupants. *Build. Environ.* 106, 237–244.
- Matawle, J.L., Pervez, S., Dewangan, S., Shrivastava, A., Tiwari, S., Pant, P., Deb, M.K., Pervez, Y., 2015. Characterization of PM<sub>2.5</sub> source profiles for traffic and dust sources in Raipur, India. *Aerosol Air Qual. Res.* 15 (7), 2537–2548.
- Mukherjee, S., Dutta, M., Ghosh, A., Chatterjee, A., 2022. A year-long study on PM<sub>2.5</sub> and its carbonaceous components over eastern Himalaya in India: contributions of

- local and transported fossil fuel and biomass burning during premonsoon. *Environ. Res.* 212, 113546.
- Nair, M., Dey, S., Bherwani, H., Ghosh, A.K., 2022. Long-term changes in aerosol loading over the 'Bihar' State of India using nineteen years (2001–2019) of high-resolution satellite data ( $1 \times 1 \text{ km}^2$ ). *Atmos. Pollut. Res.* 13 (1), 101259.
- Omar, A.H., Winker, D.M., Vaughan, M.A., Hu, Y., Trepte, C.R., Ferrare, R.A., Lee, K.P., Hostetler, C.A., Kittaka, C., Rogers, R.R., Kuehn, R.E., 2009. The CALIPSO automated aerosol classification and lidar ratio selection algorithm. *J. Atmos. Ocean. Technol.* 26 (10), 1994–2014.
- Paatero, P., Hopke, P.K., 2003. Discarding or downweighting high-noise variables in factor analytic models. *Anal. Chim. Acta* 490 (1–2), 277–289.
- Paatero, P., Hopke, P.K., Song, X.H., Ramadan, Z., 2002. Understanding and controlling rotations in factor analytic models. *Chemometr. Intell. Lab. Syst.* 60 (1–2), 253–264.
- Pakbin, P., Ning, Z., Shafer, M.M., Schauer, J.J., Sioutas, C., 2011. Seasonal and spatial coarse particle elemental concentrations in the Los Angeles area. *Aerosol. Sci. Technol.* 45 (8), 949–963.
- Pan, J., Zhou, C., Liu, C., Tang, M., Cao, S., Hu, T., Ji, W., Luo, Y., Wen, M., Zhang, N., 2018. Modes of occurrence of rare earth elements in coal fly ash: a case study. *Energy Fuel.* 32 (9), 9738–9743.
- Parrington, J.R., Zoller, W.H., Aras, N.K., 1983. Asian dust: seasonal transport to the Hawaiian islands. *Science* 220 (4593), 195–197.
- Polissar, A.V., Hopke, P.K., Malm, W.C., Sisler, J.F., 1998. Atmospheric aerosol over Alaska: 1. Spatial and seasonal variability. *J. Geophys. Res. Atmos.* 103 (D15), 19035–19044.
- Pope III, C.A., Dockery, D.W., 2006. Health effects of fine particulate air pollution: lines that connect. *J. Air Waste Manag. Assoc.* 56 (6), 709–742.
- Pope III, C.A., Burnett, R.T., Thurston, G.D., Thun, M.J., Calle, E., Krewski, D., E, Godleski, J.J., 2004. Cardiovascular mortality and long-term exposure to particulate air pollution: epidemiological evidence of general pathophysiological pathways of disease. *Circulation* 109 (1), 71–77.
- Pope III, C.A., Ezzati, M., Dockery, D.W., 2009. Fine-particulate air pollution and life expectancy in the United States. *N. Engl. J. Med.* 360 (4), 376–386.
- Rai, A., Mukherjee, S., Choudhary, N., Ghosh, A., Chatterjee, A., Mandal, T.K., Sharma, S. K., Kotnala, R.K., 2021. Seasonal transport pathway and sources of carbonaceous aerosols at an urban site of eastern Himalaya. *Aerosol Sci. Eng.* 5 (3), 318–343.
- Ravishankara, A.R., David, L.M., Pierce, J.R., Venkataraman, C., 2020. Outdoor air pollution in India is not only an urban problem. *Proc. Natl. Acad. Sci. USA* 117 (46), 28640–28644.
- Ray, D., Ghosh, A., Chatterjee, A., Ghosh, S.K., Raha, S., 2019. Size-specific PAHs and associated health risks over a tropical urban metropolis: role of long-range transport and meteorology. *Aerosol Air Qual. Res.* 19 (11), 2446–2463.
- Reff, A., Eberly, S.I., Bhave, P.V., 2007. Receptor modeling of ambient particulate matter data using positive matrix factorization: review of existing methods. *J. Air Waste Manag. Assoc.* 57 (2), 146–154.
- Roy, A., Chatterjee, A., Sarkar, C., Das, S.K., Ghosh, S.K., Raha, S., 2017. A study on aerosol-cloud condensation nuclei (CCN) activation over eastern Himalaya in India. *Atmos. Res.* 189, 69–81.
- Roy, A., Chatterjee, A., Ghosh, A., Das, S.K., Ghosh, S.K., Raha, S., 2019. Below-cloud Scavenging of Size-Segregated Aerosols and its Effect on Rainwater Acidity and Nutrient Deposition: A Long-Term (2009–2018) and Real-Time Observation over Eastern Himalaya, vol. 674. *Science of The Total Environment*, pp. 223–233.
- Sarkar, C., Chatterjee, A., Majumdar, D., Roy, A., Srivastava, A., Ghosh, S.K., Raha, S., 2017. How the atmosphere over eastern Himalaya, India is polluted with carbonyl compounds? Temporal variability and identification of sources. *Aerosol Air Qual. Res.* 17 (9), 2206–2223.
- Sarkar, C., Roy, A., Chatterjee, A., Ghosh, S.K., Raha, S., 2019. Factors Controlling the Long-Term (2009–2015) Trend of PM2. 5 and Black Carbon Aerosols at Eastern Himalaya, India, vol. 656. *Science of the Total Environment*, pp. 280–296.
- Sharma, S.K., Mandal, T.K., Jain, S., Sharma, A., Saxena, M., 2016. Source apportionment of PM2. 5 in Delhi, India using PMF model. *Bull. Environ. Contam. Toxicol.* 97 (2), 286–293.
- Sharma, S.K., Choudhary, N., Kotnala, G., Das, D., Mukherjee, S., Ghosh, A., Vijayan, N., Rai, A., Chatterjee, A., Mandal, T.K., 2020a. Wintertime carbonaceous species and trace metals in PM10 in Darjeeling: a high altitude town in the eastern Himalayas. *Urban Clim.* 34, 100668.
- Sharma, S.K., Choudhary, N., Kotnala, G., Das, D., Mukherjee, S., Ghosh, A., Vijayan, N., Rai, A., Chatterjee, A., Mandal, T.K., 2020b. Wintertime carbonaceous species and trace metals in PM10 in Darjeeling: a high altitude town in the eastern Himalayas. *Urban Clim.* 34, 100668.
- Sharma, S.K., Banoo, R., Mandal, T.K., 2021a. Seasonal characteristics and sources of carbonaceous components and elements of PM10 (2010–2019) in Delhi, India. *J. Atmos. Chem.* 78 (4), 251–270.
- Sharma, S.K., Mukherjee, S., Choudhary, N., Rai, A., Ghosh, A., Chatterjee, A., Vijayan, N., Mandal, T.K., 2021b. Seasonal variation and sources of carbonaceous species and elements in PM2. 5 and PM10 over the eastern Himalaya. *Environ. Sci. Pollut. Control Ser.* 28 (37), 51642–51656.
- Soni, K., Kapoor, S., Parmar, K.S., Kaskaoutis, D.G., 2014. Statistical analysis of aerosols over the Gangetic–Himalayan region using ARIMA model based on long-term MODIS observations. *Atmos. Res.* 149, 174–192.
- Taneja, K., Ahmad, S., Ahmad, K., Attri, S.D., 2016. Time series analysis of aerosol optical depth over New Delhi using Box–Jenkins ARIMA modeling approach. *Atmos. Pollut. Res.* 7 (4), 585–596.
- Tanner, R.L., 1982. An ambient experimental study of phase equilibrium in the atmospheric system: aerosol H<sup>+</sup>, NH<sub>4</sub><sup>+</sup>, SO<sub>2</sub>–4, NO<sub>3</sub>–NH<sub>3</sub> (g), HNO<sub>3</sub> (g). *Atmos. Environ.* 16 (12), 2935–2942, 1967.
- Turpin, B.J., Huntzicker, J.J., 1995. Identification of secondary organic aerosol episodes and quantitation of primary and secondary organic aerosol concentrations during SCAQS. *Atmos. Environ.* 29 (23), 3527–3544.
- Wang, Y., Zhuang, G., Tang, A., Yuan, H., Sun, Y., Chen, S., Zheng, A., 2005. The ion chemistry and the source of PM2. 5 aerosol in Beijing. *Atmos. Environ.* 39 (21), 3771–3784.
- Wang, Y.Q., Zhang, X.Y., Draxler, R.R., 2009. TrajStat: GIS-based software that uses various trajectory statistical analysis methods to identify potential sources from long-term air pollution measurement data. *Environ. Model. Software* 24 (8), 938–939.
- Wei, W., Cheng, S., Li, G., Wang, G., Wang, H., 2014. Characteristics of Volatile Organic Compounds (VOCs) Emitted from a Petroleum Refinery in Beijing, China, vol. 89. *Atmospheric Environment*, pp. 358–366.
- Whiteaker, J.R., Suess, D.T., Prather, K.A., 2002. Effects of meteorological conditions on aerosol composition and mixing state in Bakersfield, CA. *Environ. Sci. Technol.* 36 (11), 2345–2353.
- Winker, D.M., Vaughan, M.A., Omar, A., Hu, Y., Powell, K.A., Liu, Z., Hunt, W.H., Young, S.A., 2009. Overview of the CALIPSO mission and CALIOP data processing algorithms. *J. Atmos. Ocean. Technol.* 26 (11), 2310–2323.
- Yu, C., Wu, D., Yu, J.Z., 2019. Estimation and uncertainty analysis of secondary organic carbon using 1 year of hourly organic and elemental carbon data. *J. Geophys. Res. Atmos.* 124 (5), 2774–2795.
- Xiao, H.W., Wu, J.F., Luo, L., Liu, C., Xie, Y.J., Xiao, H.Y., 2020. Enhanced biomass burning as a source of aerosol ammonium over cities in central China in autumn. *Environ. Pollut.* 266, 115278.
- Yu, J., Yan, C., Liu, Y., Li, X., Zhou, T., Zheng, M., 2018. Potassium: a tracer for biomass burning in Beijing? *Aerosol Air Qual. Res.* 18 (9), 2447–2459.
- Yan, Y., He, Q., Guo, L., Li, H., Zhang, H., Shao, M., Wang, Y., 2017. Source apportionment and toxicity of atmospheric polycyclic aromatic hydrocarbons by PMF: Quantifying the influence of coal usage in Taiyuan, China. *Atmos. Res.* 193, 50–59.
- Yu, H., Li, W., Zhang, Y., Tunved, P., Dall'Osto, M., Shen, X., Sun, J., Zhang, X., Zhang, J., Shi, Z., 2019. Organic coating on sulfate and soot particles during late summer in the Svalbard Archipelago. *Atmos. Chem. Phys.* 19 (15), 10433–10446.
- Zhou, Y., Zheng, N., Luo, L., Zhao, J., Qu, L., Guan, H., Xiao, H., Zhang, Z., Tian, J., Xiao, H., 2021. Biomass burning related ammonia emissions promoted a self-amplifying loop in the urban environment in Kunming (SW China). *Atmos. Environ.* 253, 118138.